

Testing of Pressure Sensitive Adhesives for Transdermal Therapeutic Systems

Michael Meurer, Ph.D.

Doctoral Thesis Summary



Tomas Bata University in Zlín
Faculty of Technology

Doctoral Thesis Summary

Testing of Pressure Sensitive Adhesives for Transdermal Therapeutic Systems

Testování adheziv v transdermálních terapeutických materiálech

Author:	Michael Meurer, Ph.D.
Degree program:	P 3909 Process Engineering
Degree Course:	3909V013 Tools and Processes
Supervisor:	Prof. Ing. Berenika Hausnerová, Ph.D.
External examiners:	Doc. Petr Filip, CSc. Prof. Petr Svoboda, Ph.D.

Zlín, January 2024

© Meurer, Michael

Published by **Tomas Bata University in Zlin** in the Edition **Doctoral Thesis**

The publication was issued in the year 2024

Keywords: adhesion, rheology, pressure sensitive adhesives, transdermal therapeutic systems, diffusion

Klíčová slova: adheze, reologie, tlakově senzitivní adheziva, transdermální terapeutické materiály, difúze

Full text of the doctoral thesis is available in the Library of TBU in Zlín.

ISBN: 978-80-7678-230-3

RESUME

Traditional and newly developed testing methods were used for extensive application-related characterization of transdermal therapeutic systems (TTS) and pressure sensitive adhesives (PSA). Large amplitude oscillatory shear tests of PSAs were correlated to the material behavior during the patient's motion and showed that all PSAs were located close to the gel point. Furthermore, an increasing strain amplitude results in stretching and yielding of the PSA's microstructure causing a consolidation of the network and a release with increasing strain amplitude. *RheoTack* approach was developed to allow for an advanced tack characterization of TTS with visual inspection. The results showed a clear resin content and rod geometry dependent behavior, and displays the PSA's viscoelasticity resulting in either high tack and long stretched fibrils or non-adhesion and brittle behavior. Moreover, diffusion of water / sweat during TTS's application might influence its performance. Therefore, a dielectric analysis based evaluation method displayed occurring water diffusion into the PSA from which the diffusion coefficient can be determined, and showed clear material and resin content dependent behavior. All methods allow for an advanced product-oriented material testing that can be utilized within further TTS development.

RESUMÉ IN CZECH

Tradiční a nově vyvinuté testovací metody byly použity pro rozsáhlou charakterizaci transdermálních terapeutických systémů (TTS) a adheziv citlivých na tlak (PSA). Měření PSA v LAOS (Large Amplitude Oscillatory Shear) režimu korelovala s chováním materiálu při pohybu pacienta a ukázala, že všechna PSA se nacházejí v blízkosti bodu gelace. Zvyšování amplitudy deformace má navíc za následek roztahování a poddajnost mikrostruktury PSA, což způsobuje nejprve konsolidaci sítě a následně její uvolnění s rostoucí amplitudou deformace. V rámci disertační práce byla vyvinuta nová metoda *RheoTack*, která umožňuje pokročilou charakterizaci přilnavosti TTS s vizuální kontrolou během měření. Výsledky *RheoTack* ukázaly zřetelně vliv obsahu pryskyřice i geometrie nástroje. Vysoké adhezní hodnoty jsou spojeny s protaženými fibrilami těchto viskoelastických materiálů, nepřilnavost znamená naopak křehký lom. Difúze vody nebo potu během aplikace TTS může ovlivnit jejich výkonnost. Proto byla difúze vody do PSA hodnocena pomocí metody založené na dielektrické analýze. Získané difúzní koeficienty ukázaly jasné rozdíly v závislosti na materiálu a obsahu pryskyřice. Navržené a otestované metody umožňují pokročilé hodnocení materiálů orientované na aplikaci, které lze využít v rámci dalšího vývoje TTS.

ABSTRACT

Transdermal therapeutic systems (TTS) are medical patches for the systematic treatment of e.g. severe pain, Parkinson or Alzheimer disease by releasing active pharmaceutical ingredients through the human skin. For successful medication, good adhesion of the TTS starting from the application on the patient's skin, during the application time 12 hours to 7 days taking patient's sweating, movement and friction into account, and traumaless removal from the skin are required. To fulfill these requirements, development of TTS is based on standardized testing methods taken from technical bonding for short- and long-term adhesion characterization. Unfortunately, these testing methods do not provide suitable information about the high requirements of TTS behavior on human skin.

This thesis addresses short and large amplitude oscillatory shear measurements of pressure sensitive adhesives (PSA) which can be correlated the patient's movement. Moreover, a dielectric analysis based method was developed, investigating diffusion kinetics of water diffusing into PSA. Further, new tack testing approach called *RheoTack* was developed, and implemented on a plate-plate rotational rheometer for tack testing of TTS.

The large amplitude oscillatory shear measurements can be related to deformation states which TTS experiences during daily life motion of a patient. These results showed that the investigated PSAs were located close to the gel point and that increasing strain amplitudes caused a consolidation of the gelled network, being stretched and released with a further increase of the strain amplitudes. Evaluation of the elastic and viscous Lissajous Bowditch diagrams revealed that a higher resin content caused higher shear thickening and shear thinning effects which resulted in a considerably more yielded and stretched microstructure of the PSA.

The influence of water and isotonic NaCl solution on the ion/dipole mobility was recorded with dielectric analysis, showing that this diffusion process was dependent on the PSA's chemical composition, the resin content with its resulting free volume in the PSA, and the diffusant itself. From these measurements, the diffusion coefficient can be determined being in accordance with literature values.

Newly developed *RheoTack* approach allows for an extensive characterization of the adhesion and release behavior of TTS together with a visual inspection of occurring detaching processes. Quantitative data evaluation showed that PSA type, resin content, retraction speed, and rod geometry influenced *RheoTack*

parameters of TTS clearly. Extensive fibrillation and high tackiness were recorded for lower retraction speeds with lower resin contents, while brittle failure with non-tackiness was observed for higher retraction speeds and resin contents.

Furthermore, for the flat rods the highest stresses occurred at the circumferential stripe, while the center exhibited the highest stresses for the rounded rod. This stress differences caused contrasting release behavior, resulting in one force maxima for the flat rods, while the rounded rod reveals a plateau or a second force maxima. This displays that the rod geometry influences the tack behavior clearly.

The results from these developed testing methods give a better and more comprehensive insight into the PSA's and the TTS's material performance, leading to an approved application-related characterization than from standardized methods. As a result, this new knowledge contributes to further TTS development, and a higher livability for the patients.

CONTENT

Resume	3
Resumé in Czech	3
Abstract.....	4
1 State of the Art.....	8
1.1 Introduction.....	8
1.1.1 PSAs for medical patches – TTS.....	9
1.1.2 Production of TTS	10
1.2 Methods to determine adhesive properties	11
1.3 Methods to determine rheological properties	12
1.4 Methods to determine diffusion properties.....	14
2 Aim of the Work.....	16
3 Materials and Methods	18
4 Discussion of the Results	20
4.1 Rheological properties – shearing of PSA and TTS.....	20
4.1.1 Amplitude sweeps of PSAs within short amplitude oscillatory shear [36] 20	
4.1.2 Rheological characterization of PSA within large amplitude oscillatory shear [36]	22
4.2 Diffusion properties [37]	25
4.2.1 Diffusion into PSA monitored with DEA [37]	25
4.3 Adhesion properties	31
4.3.1 Standardized tests – probe tack and shear strength.....	31
4.3.2 RheoTack development [38]	32
4.3.3 RheoTack data evaluation and results [38]	33
5 Conclusion.....	42
6 Contribution to Science and Practice	43
References	45
List of Figures	49
List of Tables.....	51

Abbreviations	52
Publications, Posters and Presentations	54
Curriculum Vitae	55

1 STATE OF THE ART

1.1 Introduction

Transdermal therapeutic systems (TTS) are medical patches basing on pressure sensitive adhesives (PSA) which contain active pharmaceutical ingredients (API) and are applied to the patients' skin who suffer from e.g. severe pain, Parkinson or Alzheimer. TTS are advantageous for patients due to a better compliance, a continuous drug level in a blood system, and therefore friendly for the patient's stomach [1].

TTS are categorized in drug-in-adhesive matrix and drug reservoir type, **Fig. 1**. The first patch consists of a protective backing membrane, a drug-in-adhesive layer and a release liner. The drug-in-adhesive layer controls both the adhesion on and the drug release into the skin. The second patch contains an additional drug reservoir, a semi permeable membrane and a contact adhesive layer. While skin adhesion is secured by the contact adhesive layer, the API release from the reservoir is controlled by the semi-permeable membrane.

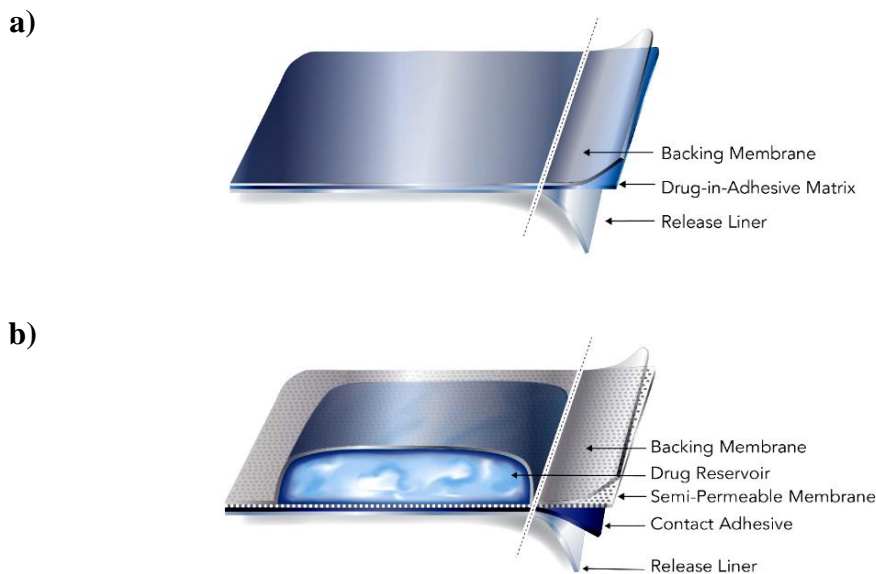


Fig. 1: Design of transdermal therapeutic systems (TTS) – a) drug-in-adhesive matrix type and b) drug reservoir type [2].

A continuous release of the API through the patient's skin leads to a uniform level of API in the blood system. Currently, the application time of 12 h to 7 days represents a challenge for the PSA as e.g. detaching of the patch may cause an uncontrolled medicine release and "cold flow" due to the static low viscosity flow of the PSA from underneath the backing layer. The successful application of

patches on the patient's skin requires adhesion of the entire TTS for the complete application time as well as a traumaless and easy removal afterwards [3].

1.1.1 PSAs for medical patches – TTS

Soft Polymers used for PSAs are acrylates, polyisobutylene, silicones and their mixtures [4]. The use of a PSA on a skin is performed by applying slight pressure to attach to skin and is to be removed without a residue. Thus, the requirements of an appropriate adhesion consist of good flowability and wetting of the PSA towards the substrate surface. Additionally, the residue-free removal demands sufficiently stiff behavior and cohesion of the PSA. Hence, during the application time the entire TTS has to follow the skin motions without detaching to guarantee a successful medication [3, 5]. Considering the complex requirements of PSAs for TTS, the pros and cons of the most important criteria are presented in **Table 1**.

Table 1: Pros and cons of PSAs that are used for TTS [6-8].

	Acrylates	Polyisobutylenes	Silicones
Pro's	good adhesion properties	high tack weak adhesive properties	adhesion towards surfaces having a low surface energy
	good resistance towards aging	good thermal stability good oxidative stability good chemical resistance	good chemical resistance low chemical reactivity and toxicity good temperature stability
	high vapor transmission		high gas and vapor permeability
		low toxicity no skin irritation	low skin irritation and sensitizing
	relatively cheap		
Con's	low adhesion to surfaces with low surface energies	bad adhesion to many surfaces due to low polarity	lower adhesion strength than comparable organic PSAs
	skin irritation and sensitizing	costly production process of final products	costly flourosiliconated release liner necessary
		low air, moisture and gas permeability	

Silicone PSAs consist of linear high molecular weight silicone polymers and highly branched silanol functional siloxane resins, having a complex three dimensional structure [5, 6]. The polymer and resin are chemically cross-linked during a base-catalyzed polycondensation reaction through the silanol functionalities on the resin and the terminal silanols of the polymer.

The non-amine compatible (NAC) PSA, the result of a “bodying process”, is a broad network consisting of polymer chains connected to resin molecules with OH- groups at the end of the polymer chains, **Fig. 2**. A further chemical treatment of the NAC leads to the amine compatible (AC) PSA having inert trimethylsilyl end groups, which prevent possible reactions between PSA and API [5, 6].

Silicone PSAs are well suited for applications as TTS due to their appropriate properties for medical usage. Their low toxicity towards skin, the low chemical reactivity with respect to API and skin, and the excellent chemical resistance towards acids or bases and the environmental stability with respect to moisture make them suitable for skin applications. Although silicone PSAs have fairly good adhesion properties to many substrates, the final adhesion strength of organic PSAs are higher. Besides higher material prices for silicone PSAs, special and expensive flourosiliconised release liners are necessary to enable easy removal of the backing layer from the silicone PSAs. Based on these arguments, especially the low toxicity for skin applications, silicone PSAs were chosen for this work.

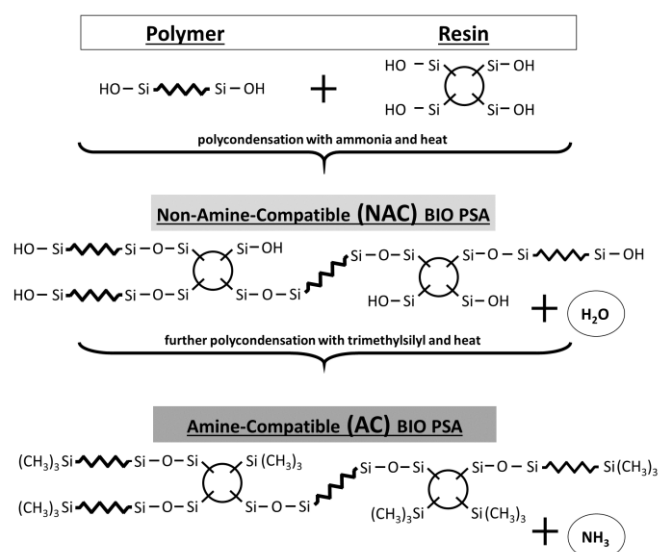


Fig. 2: Chemical structures of the non-amine compatible (NAC) and amine-compatible (AC) PSA and the steps of their synthesis (according to [9]).

1.1.2 Production of TTS

The production of TTS is a multistage process that starts with the mixing of the dissolved PSA in a system related organic solvent with the API. The concentration of the API is close to the maximum solubility limit.

After the mixing process, the drug containing adhesive mixture is introduced to the coating process consisting of the following steps, **Fig. 3**:

- a) drug containing adhesive mixture is coated on the release liner by a doctor roll at the coating head
- b) the adhesive film is dried in the drying channel
- c) the backing layer is attached onto the adhesive system
- d) the adhesive system is rolled to master rolls for further processing.

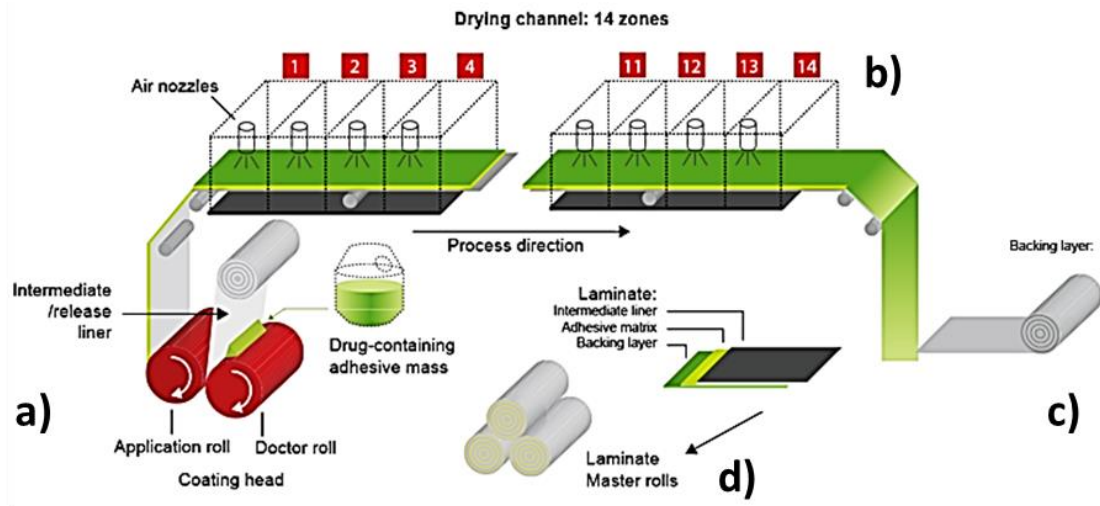


Fig. 3: Scheme of TTS manufacturing with a coating head, drying- and laminating zone [10].

The final step of the TTS production is the cutting and packaging to single pouches. The production of these medical patches demands high standards according to e.g. Transdermal and Topical Delivery Systems – Product Development and Quality Considerations FDA [2], EMA [11], ICH Q8(R2) [12] and ICH Q2(R1) [13], and requires clean rooms to avoid contaminations.

1.2 Methods to determine adhesive properties

Most measuring techniques and standardized testing methods which characterize adhesion behavior originate from adhesive bonding, are performed mainly on stainless steel substrates and are also used for quality assurance purposes of TTS.

The short-term adhesion behavior of patches is determined by either probe tack test according to ASTM D2979 [14], or loop tack test according to DIN EN 1719 [15].

Peel adhesion properties of patches are determined on stainless steel plates according to DIN EN ISO 29862 [16] with angles either 90° or 180°.

Static shear test characterizes the uniformity of adhesion properties of patches by measuring the time to failure according to DIN EN ISO 29863 [17].

1.3 Methods to determine rheological properties

During the manufacturing the dissolved PSA experiences (mixing process and the coating of the dissolved PSA onto the release liner) shear flow and extensional flow. Whereas, during the TTS's application the solid-like PSA is subjected to shear flow stresses. When removed from a skin, both extensional and shear stress occur in different ratios depending on the peel-off angle and retraction velocity.

The short amplitude oscillatory shear (SAOS) rheology measurement, **Fig. 4a**), according to DIN EN ISO 53019-4 [18] allows for standardized determination of viscoelastic properties as a function of temperature and frequency of fluids, gels and soft solids. Viscoelastic materials exhibit a phase shift between sinusoidal excitation and sinusoidal response, **Fig. 4 b**).

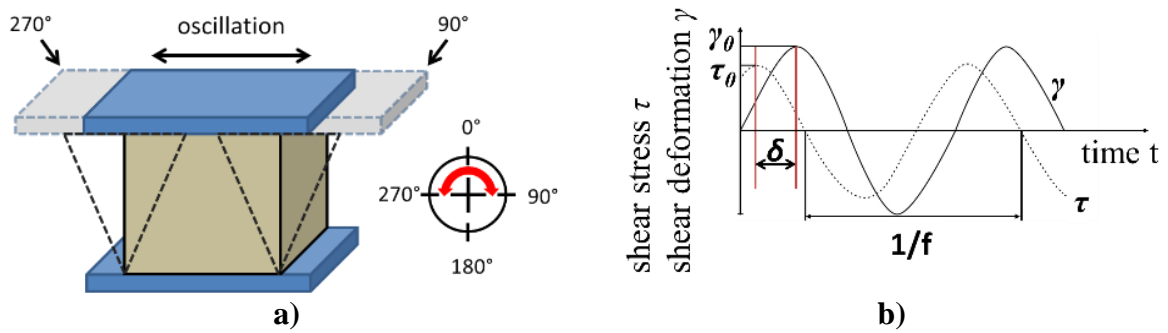


Fig. 4: Scheme of the oscillatory shear measurement a) sample is loaded in an oscillatory manner between two plates, b) sinusoidal excitation (γ), response signal (τ) and phase angle (δ).

The deformation $\gamma(\omega, t)$ is given by

$$\gamma(\omega, t) = \gamma_0(\omega) \sin(\omega t) = \gamma_0 * e^{i(\omega t)} \quad (1)$$

with frequency ω and deformation amplitude $\gamma_0(\omega)$. The stress response is

$$\tau(\omega, t) = \tau_0(\omega) \sin(\omega t + \delta(\omega)) = \tau_0 * e^{i(\omega t + \delta(\omega))} \quad (2)$$

This yields the complex shear modulus G^* :

$$G^*(\omega, \delta) = \frac{\tau_0(\omega) * e^{i(\omega t)} * e^{i(\delta)}}{\gamma_0(\omega) * e^{i(\omega t)}} = \underbrace{G_0(\omega) \cos(\delta(\omega))}_{\text{storage modulus } G'} + i \underbrace{G_0(\omega) \sin(\delta(\omega))}_{\text{loss modulus } G''} \quad (3)$$

The real part of G^* represents the storage modulus G' , which is a measure of the elastically stored energy, and the imaginary part of G^* represents the loss modulus G'' , which is a measure of the dissipated energy. A further important quantity is the loss factor characterizing the damping behavior:

$$\tan \delta(\omega) = \frac{G''}{G'} \quad (4)$$

With increasing shear amplitude, the originally sinusoidal stress becomes distorted indicating the end of the linear viscoelastic region (LVE), where G' and G'' are independent of the applied strain amplitude γ_0 . This end is determined by an amplitude sweep at constant frequency and temperature, **Fig. 5**. At higher amplitudes G' and G'' decrease.

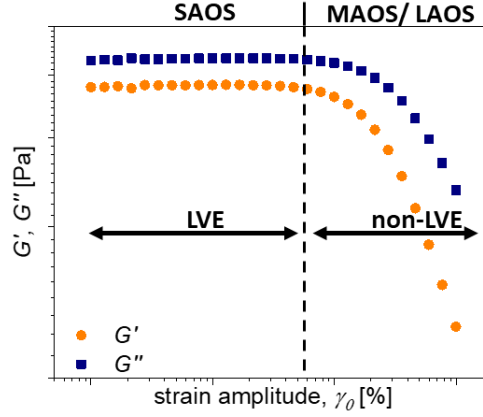


Fig. 5: G' and G'' being independent from strain amplitude γ_0 in the LVE / SAOS and dependent from the strain amplitude γ_0 in the middle and large amplitude oscillatory shear region (MAOS, LAOS).

Using frequency sweeps, the viscoelastic properties of PSAs can be determined over a frequency range of 4 to 6 orders of magnitude. At low frequencies, G' and G'' can be correlated to peel adhesion and tack during bonding and at high frequencies to peel adhesion and tack during debonding or detaching [19].

Large amplitude oscillatory shear (LAOS) measurement allows for the determination of rheological behavior beyond the LVE range and is a relevant method for materials which are subjected to large and fast deformations. The non-sinusoidal character of the response signal requires data evaluation by Fourier analysis providing relevant intensities in terms of higher harmonics. In the SAOS range only the 1st harmonic I_1 is not zero, while in MAOS the 3rd harmonic I_3 becomes relevant and in the LAOS range there may occur 5th and 7th harmonics. Therefore, the ratio $I_{3/1}$ is used as a measure of a nonlinear behavior.

Strain amplitude dependent moduli G' and G'' can also be evaluated in the LAOS range using Lissajous-Bowditch diagrams, **Fig. 6**. Therefore, inter-cycle (between different γ_0) and intra-cycle (within a cycle) nonlinear behavior is characterized by the quantities:

$$\text{Zero-strain modulus} \quad G'_M(\gamma) = \left. \frac{d\sigma}{d\gamma} \right|_{\gamma=0} \quad (5)$$

$$\text{Maximum-strain modulus} \quad G'_L(\gamma) = \left. \frac{\sigma}{\gamma} \right|_{\gamma=\pm\gamma_0} \quad (6)$$

$$\text{Zero-rate dynamic viscosity} \quad \eta'_M(\dot{\gamma}) = \left. \frac{d\sigma}{d\dot{\gamma}} \right|_{\dot{\gamma}=0} \quad (7)$$

$$\text{Maximum-rate dynamic viscosity} \quad \eta'_L(\dot{\gamma}) = \left. \frac{\sigma}{\dot{\gamma}} \right|_{\dot{\gamma}=\pm\dot{\gamma}_0} \quad (8)$$

γ_0 strain amplitude, $\dot{\gamma}(t)$ the time dependent shear rate and $\dot{\gamma}_0$ the shear rate amplitude. These quantities can be used to define further LAOS quantities:

$$\text{Strain stiffening ratio} \quad S(\gamma_0) \equiv \frac{G'_L(\gamma_0) - G'_M(0)}{G'_L(\gamma_0)} \quad (9)$$

$$\text{Shear thickening ratio} \quad T(\gamma_0) \equiv \frac{\eta'_L(\dot{\gamma}_0) - \eta'_M(0)}{\eta'_L(\dot{\gamma}_0)} \quad (10)$$

$S > 0$ indicates intra-cycle strain stiffening behavior and $S < 0$ intra-cycle strain softening behavior. The $T > 0$ indicates intra-cycle shear thickening behavior and $T < 0$ intra-cycle shear thinning behavior. If $S = 0$ and $T = 0$, the material behaves linear viscoelastic.

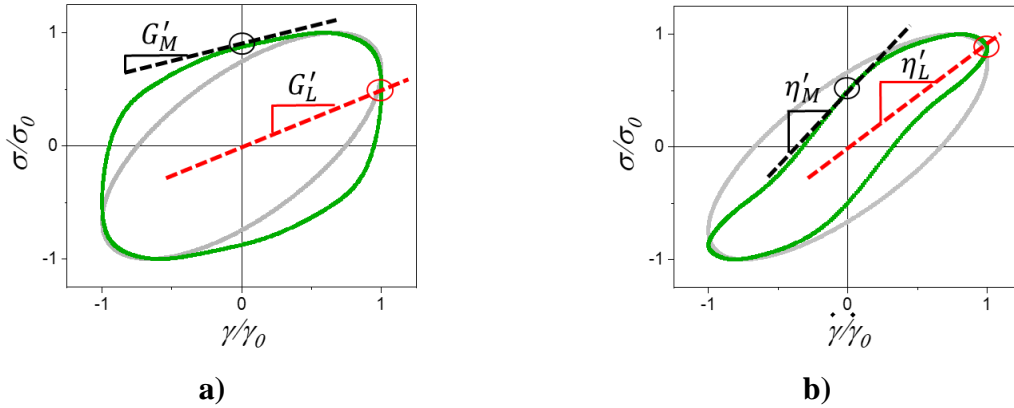


Fig. 6: Normalized elastic a) and viscous b) Lissajous-Bowditch diagrams for linear viscoelastic behavior (light grey) and nonlinear behavior (green) with determination of zero-strain modulus G'_M , maximum strain modulus G'_L , zero-rate dynamic viscosity η'_M , and maximum-rate dynamic viscosity η'_L .

1.4 Methods to determine diffusion properties

Diffusion describes processes in which matter is transported from one part of a system to another by random molecular motions. The first mathematical description of diffusion was postulated by Fick in 1855 [20]. The permeation process through polymers consists of three steps:

- sorption of the diffusing substance at the contact surface,
- diffusion through the polymer due to the concentration gradient,
- desorption and evaporation of the diffusing substance at the other surface

Common methods to investigate diffusion and permeation behavior are time lag experiments, sorption experiments, chromatographic experiments, and dielectric analysis (DEA) [21-24].

The dielectric analysis (DEA) allows for monitoring of dielectric changes of polymers e.g. during crosslinking of thermosets or to analyze diffusion processes within polymeric materials [24, 25]. The sample is exposed to an alternating external electric field forcing ions to move and dipoles to orientate with respect to this field. Both effects are linked to dissipation of energy due to internal friction. The investigated quantity during monitoring resin curing processes or diffusion experiments is the frequency dependent ion viscosity η^{ion} being the reciprocal to the ion conductivity σ :

$$\eta^{ion}(f) = \frac{1}{\sigma(f)} = \frac{1}{2\pi f \varepsilon_0 \varepsilon''(f)} \quad (11)$$

with frequency f , dielectric loss ε'' and dielectric constant ε_0 [26, 27]. Several researchers [24, 28-30] reported that the ion viscosity η^{ion} can be used to investigate diffusion processes as it is sensitive to changes of macromolecule mobility and ion concentration. Both are affected if low molecular substances diffuse into PSA. Therefore, the measured η^{ion} is related to the diffusion coefficient. Wittchen et al. [24] derived:

$$\log \eta^{ion}(t) = \log A_0 + \frac{B'}{1 - \frac{V_g}{M_\infty \frac{8}{\pi^2} \exp\left(-\frac{D\pi^2 t}{4l^2}\right) + \frac{\rho_{solV}}{V_g}}} \quad (12)$$

where A_0 is pre-exponential factor, B' represents fractional free volume being relevant for mobility and transport, V_g is volume of dry coating, M_∞ stands for amount at infinite time, D is diffusion coefficient and ρ_{solV} is density of the solvent. They verified eq. 22 for swelling polyurethane coatings with respect to temperature and composition, **Fig. 7**.

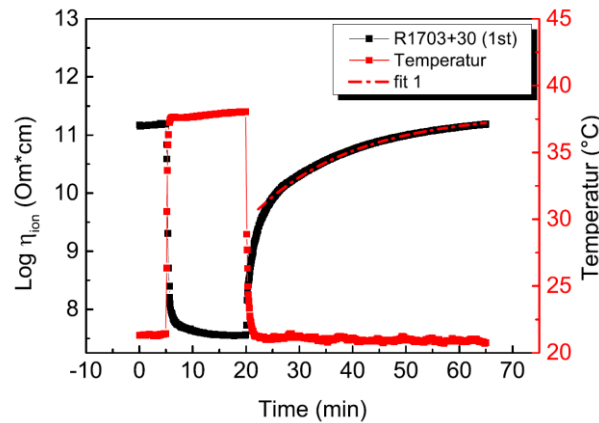


Fig. 7: Effect of temperature on the ion viscosity during desorption [24].

2 AIM OF THE WORK

The medical transdermal therapeutic system (TTS) consists of pressure sensitive adhesive (PSA) containing active pharmaceutical ingredient (API) and a protective backing layer, and have to meet high and often opposing requirements arising from a multi-day application time and a traumaless removal.

Standardized testing methods adopted from technical bonding to characterize short- and long-term adhesion of TTS use stainless steel or aluminum plates. This does not correspond to application conditions of TTS with respect to adhesion and detaching processes on skin. As a consequence, these methods represent only quality assurance tools and are not capable to provide information about the TTS behavior on human skin (or polymer substrates). Furthermore, it is known that the surface properties and texture of skin differ significantly between human individuals, thus, bad instantaneous adhesion on skin or detaching during the application may endanger the therapy. Therefore, the aim of this work is the development of application related and tailor-made characterizing and testing methods for TTS with the focus on:

- development of a testing approach to determine adhesion and detaching of PSA/TTS
- viscoelastic properties of PSA/TTS subjected to small and large deformations
- determination and evaluation of the diffusion behavior of water-based liquids into the PSA, also considering cross-interactions with API and their effects on the viscoelastic properties.

The viscoelastic properties at application-relevant frequencies determine the adhesion and detaching behavior of PSA (investigated by SAOS measurements). For high skin motion, LAOS can be used to correlate the adhesive behavior at large deformation amplitudes. As standardized testing methods are not sufficient to characterize application relevant adhesion behavior, a new testing approach has to be developed regarding the stiffer and flexible backing layer.

The dielectric analysis using IDEX sensors allows for the investigation of the diffusion behavior of e.g. water under conditions close to application.

The long-term goal of this work is to provide a methodology of an application-related TTS characterization leading to the development of individualized medical patches with optimized performance resulting in safer TTS products.

The presented results are also summarized in the following publications:

- I** Michael Meurer, Roland Kádár, Esther Ramakers-van Dorp, Bernhard Möglinger, Berenika Hausnerová, **Nonlinear oscillatory shear tests of pressure-sensitive adhesives (PSAs) designed for transdermal therapeutic systems (TTS)**. *Rheol. Acta* 2021, 60, 553–570.
- II** Michael Meurer, Tim Prescher, Esther Ramakers-van Dorp, Bernhard Möglinger, Berenika Hausnerová, **RheoTack—An approach to investigate retraction rate dependent detaching behavior of pressure sensitive adhesives**. *J. Rheol.* 2022, 66, 505-514.
- III** Michael Meurer, Gatien Kamsu, Christian Dresbach, Esther Ramakers-van Dorp, Bernhard Möglinger, Berenika Hausnerová, **Rate dependent tack behavior of silicone-based pressure sensitive adhesives for transdermal therapeutic systems**.
Submitted to *J. ind. Eng. Chem.* November 2023.
- IV** Michael Meurer, Lucca Retterath, Esther Ramakers-van Dorp, Bernhard Möglinger, Berenika Hausnerová, **Effects of resin content on water diffusion in two chemically different silicone based pressure sensitive adhesives (PSA) using dielectric analysis (DEA)**.
Submitted to *APL Biong.* December 2023.

3 MATERIALS AND METHODS

Materials used in this study were commercially available amine-compatible (AC) and non-amine compatible (NAC) silicone PSA's (DuPont and Dow Health Care Solutions.) with resin contents between $v_F = 49.1$ and 54.2 Vol% and mixtures of it according to **Table 2**.

Table 2: Composition of PSA samples used [31-34].

Amine compatible (AC)			Non-amine compatible (NAC)		
ratio BIO PSA 4201:4301	Weight content (%)	Volume content (%)	ratio BIO PSA 4501:4601	Weight content (%)	Volume content (%)
100:0	60.00	54.2	100:0	60.00	54.2
75:25	58.75	52.9	-	-	-
50:50	57.50	51.6	50:50	57.50	51.6
25:75	56.25	50.4	-	-	-
0:100	55.00	49.1	0:100	55.00	49.1

PSA laminates of these compounds with a thickness of (150 ± 15) μm were produced on a release liner by using a coating box. These PSA layers were either laminated with a second release liner or a Polyethylene terephthalate (PET)/ Ethylene vinyl acetate (EVA) backing layer (3M Scotchpak™ 9732) [35], resulting in AC- and NAC-PSA or AC- and NAC-TTS samples, respectively.

Testing of the PSA / TTS characteristic properties was performed with the following methods and measuring devices, **Table 3**:

Table 3: Measured properties, determined quantities, tested samples and instruments.

Category/ property	Measured quantity	Tested sample	Instrument
Probe Tack [14]	F	TTS	Polyken Probe Tack Tester (ChemInstruments, Fairfield, USA)
	According to ASTM D2979 [14] with stainless steel plate $\varnothing = 5$ mm		
Peel adhesion strength [16]	$F(t)$	TTS	ZwickRoell Z005 with force transducer Zwick 100 N (Zwick, Ulm, Germany)
	According to DIN EN ISO 29862 [16] in 180 °. Sample application by hand + 2 kg roll, dwell time = 1 min, $v_{\text{retract}} = 300$ mm/s		
Rheology – amplitude sweeps (SAOS/LAOS) [36]	$G'(\gamma_0); G''(\gamma_0);$ $I_{3/1}(\gamma_0); S(\gamma_0); T(\gamma_0)$	PSA	MCR702 TwinDrive® (Anton Paar, Austria)
	Plate-plate $\varnothing = 15$ mm; $T = 30$ °C; $\omega = 0.6, 1, 2, 4$ rad/s, axial initial compression force $F = 5$ N for 15 s, released to 0 N, relaxation time 600 s for $v_F = 49.1$ to 50.4 %; 900 s for $v_F = 51.6$ to 54.2 %		
Diffusion kinetics [37]	$\eta^{\text{ion}}(t)$	PSA	DEA288 Ionic (NETZSCH Gerätebau, Germany)
	Sample thickness = 300, 600, 900 μm ; $T = 30$ °C; $f = 10$ Hz; diffusants: deionized water and 0.9 % NaCl solution		
Water absorption [37]	m (H ₂ O; 0.9 % NaCl)	PSA	Mettler Toledo AX205 DeltaRange (MettlerToledo, Columbus, USA)
	Sample size: 20 x 40 x 0.6 mm ³ ; 24 h drying step at 80 °C; 24 h immersion at 30 °C in deionized water and 0.9 % NaCl solution		
Glass temperature, thermal expansion [37]	$T_g; \alpha_{L,G}; \alpha_{L,L}$	PSA	DMA 242 E Artemis (NETZSCH Gerätebau, Germany)
	Tension; sample = 6.5 x 12 x 1 mm ³ ; clamping 10 mm; $f = 1$ Hz; dynamic ampl. 25 μm ; max. force 10.9 N; T -range = -170 to 80 °C with 2 K/min and 40 min isothermal step at -170 °C; $T_g = \text{max. of } \tan(\delta)(T)$		
RheoTack [38, 39]	$F(h)$	TTS	Haake MARS III (Thermo Fischer Scientific, USA)
	Tension & compression; geometries: plates with $\varnothing = 5$ mm (P5) and $\varnothing = 8$ mm (P8); spherical rounded rod $\varnothing = 5$ mm & $D_{\text{sphere}} = 12$ mm (R5); lower plate = TMP with borehole; $v_{\text{retract}} = 0.01, 0.1$ and 1 mm/s		

4 DISCUSSION OF THE RESULTS

4.1 Rheological properties – shearing of PSA and TTS

TTS are applied to human skin between 1 and 7 days, where they are subjected to small and large deformations [40-42]. Therefore, an application-related rheological frequency dependent characterization of the PSA in the short and large amplitude oscillatory shear regions was performed.

4.1.1 Amplitude sweeps of PSAs within short amplitude oscillatory shear [36]

Amplitude sweeps in the short amplitude oscillatory shear (SAOS) region allow for the determination of the viscous- and gel- or solid-like material behavior, as well as the ν_F -dependent shear moduli and the range of the linear viscoelastic region (LVR). **Fig. 8** shows amplitude sweeps of the PSAs with various ν_F . Both PSAs exhibit increasing moduli with increasing ν_F and a transition from solid-like ($G' > G''$) to viscous-like behavior ($G'' > G'$) within the measuring range [36].

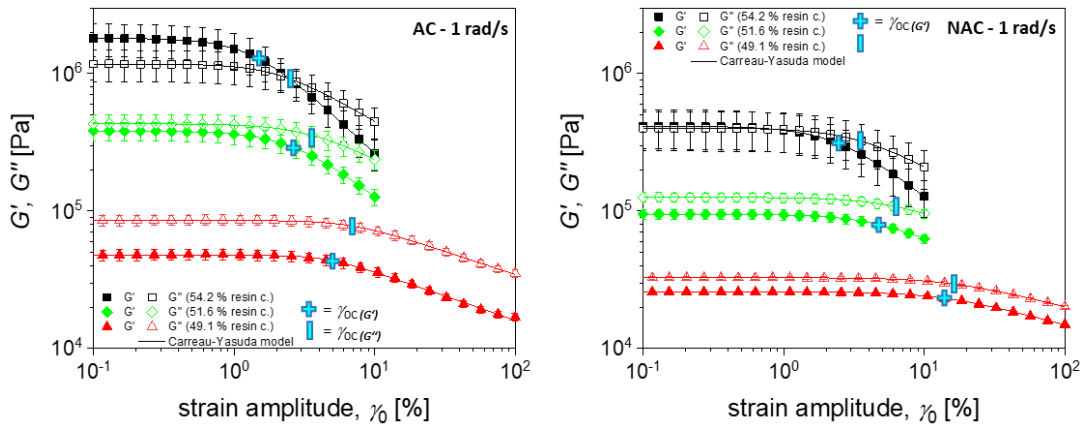


Fig. 8: Strain amplitude dependent storage G' and loss moduli G'' of AC- and NAC-PSAs for $\omega = 1$ rad/s; symbols = measured data; lines = Carreau-Yasuda-like fits [36].

The amplitude sweep curves, **Fig. 8**, allow for fitting according to the Carreau-Yasuda like model:

$$G'(\gamma_0) = G'_0(1 + (C_1\gamma_0)^{C_2})^{\frac{(C_3-1)}{C_2}} = G'_0 \left(1 + \left(\frac{\gamma_0}{\gamma_{0c}}\right)^{C_2}\right)^{\frac{(C_3-1)}{C_2}} \quad (13)$$

$$G''(\gamma_0) = G''_0(1 + (C_1\gamma_0)^{C_2})^{\frac{(C_3-1)}{C_2}} = G''_0 \left(1 + \left(\frac{\gamma_0}{\gamma_{0c}}\right)^{C_2}\right)^{\frac{(C_3-1)}{C_2}} \quad (14)$$

with G' as the storage modulus, G'' as the loss modulus and the parameter C_1 , which represents the transition from the linear to the nonlinear viscoelastic region.

C_2 stands for the range of the transition factor for strain amplitudes from the end of the linear region to the beginning of the strain amplitude-dependent decrease. The factor C_3 defines the strain amplitude dependency of G' and G'' within the nonlinear range. As G' and G'' decrease at higher strain amplitudes, according to the rheological interpretation of Sim et al. [43], the strain amplitude curves can be classified as type I, which is commonly reported for polymer melts or solutions.

The ν_F -dependent gel point can be estimated at $\approx 51.6\%$ (2 rad/s) for AC- and at 54.1% (1 rad/s) for NAC-PSAs, [36]. Furthermore, AC- exhibits a two to four times higher G'_0 than NAC-PSAs, which can be explained by the second polycondensation step for the end-group replacement from $-\text{OH}$ to $-\text{CH}_3$, resulting in higher intermolecular interactions and a higher crosslinking density.

From the linear viscoelastic point of view, nonlinear behavior is reached when moduli are dependent on the applied strain amplitude at $\gamma_{0C} < 1/C_1$. For the PSAs, γ_{0C} displays an increasing behavior with decreasing ν_F , whereas γ_{0C} of G'' exceeds those from G' . This can be explained by the decreasing ν_F , thus causing a lower crosslinking degree, lower molecular masses and reduced internal friction which increases the linear viscoelastic range for G' and G'' .

Chang und Dahlquist evaluation [36]

The linear viscoelastic data allows for the representation according to Chang [45] and Dahlquist [46], which shows that the frequency-dependent data pairs (G' , G'') lay on master curves starting in the liquid phase (data points below the $\tan(\delta)=1$ line) and end up in the solid state (data points above the $\tan(\delta)=1$ line), **Fig. 9**. As the slope of the AC-PSA master curve is higher than that for NAC-PSA, the viscoelastic properties of AC-PSA vary more. Furthermore, the Dahlquist criterion line represents an estimation of the gel point as the master curves cross the Dahlquist and the $\tan(\delta)=1$ lines in the same moduli range.

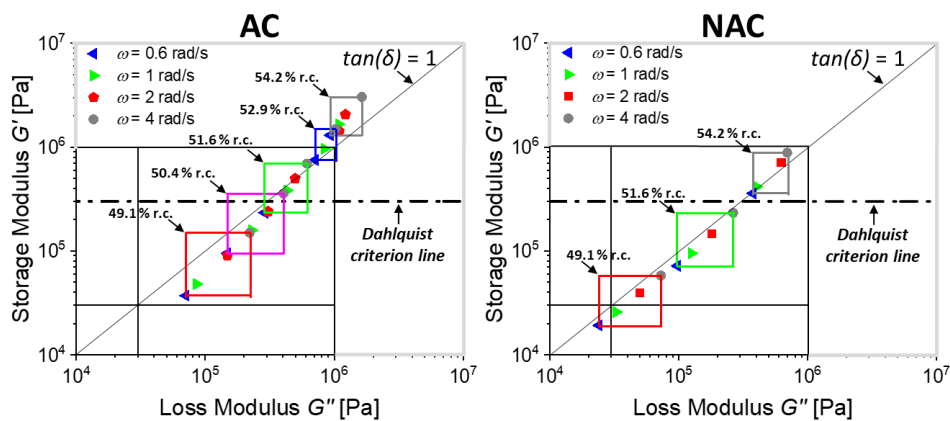


Fig. 9: Representation according to Chang and Dahlquist of SAOS data from AC- and NAC-PSAs [36].

4.1.2 Rheological characterization of PSA within large amplitude oscillatory shear [36]

In the MAOS and LAOS range, beyond the LVE, the non-sinusoidal character of the response signal contains contributions of the higher harmonics as the 3rd (I_3), 5th (I_5) and 7th (I_7). The ratio $I_{3/1}$ represents a measure for the nonlinear behavior and shows a slope of $n = -1$ due to instrument noise [47] within the SAOS range until it increases in the MAOS range with a slope between $n = 1.6$ to 2.3 , **Fig. 10**. The frequency dependent nonlinear “oddities” between the instrument noise and the MAOS region range between a slope of $n = 0$ for AC-PSAs and a local maximum. Especially NAC-PSAs exhibit strong local maxima, **Fig. 10**. As $I_{3/1}$ slopes with $n = 0$ have been reported as early evidence for consolidation of percolated networks or gelation in suspensions [48], local maxima have not been reported yet, but indicate possible molecular processes as stretching or release of physical cross-links which are not accessible in SAOS rheology.

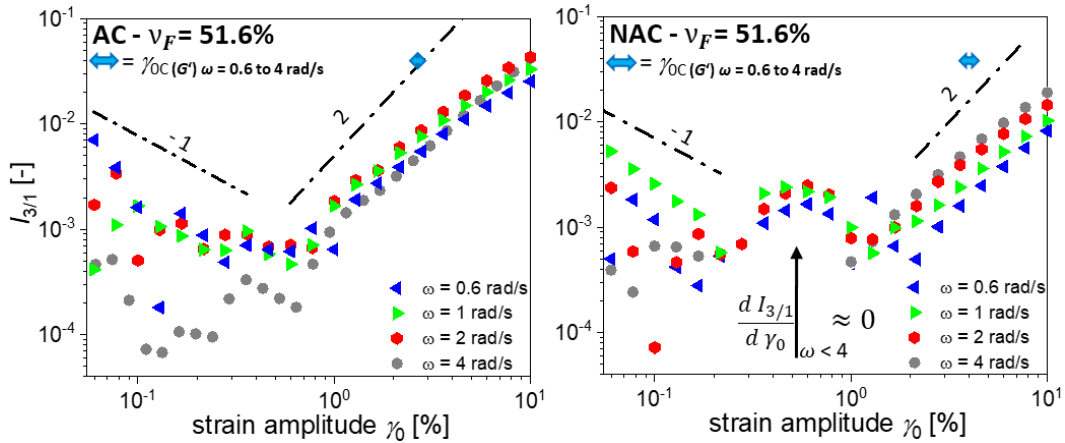


Fig. 10: Strain amplitude dependent nonlinear parameter $I_{3/1}$ (γ_0) for AC- and NAC-PSAs [36].

Intra-cycle quantification from monitored shape changes of the elastic and viscous Lissajous-Bowditch diagrams, results in the strain stiffening S and shear thickening T ratio, which are both approximately $S = T = 0$ for all AC- and NAC-PSAs within the linear viscoelastic range, **Fig. 11 and 12**. The onset of both parameters $S, T \neq 0$ where nonlinear behavior occurs can be detected at higher strain amplitudes than the limit of the LVE (determined from G' and G'') but is lower than from the $I_{3/1}$ data. Furthermore, the onset of the parameters $S, T \neq 0$ where intra-cycle nonlinearity occurs decreases with increasing ν_F , due to a reduced chain mobility, which was also found by other researchers [48-54]. The parameter S for AC-PSAs show a frequency dependency, a maximum and a wave-like response for $\nu_F = 49.1\%$, while the maxima is shifted to lower strain

amplitudes with increasing v_F and frequency. For higher v_F , maxima may be assumed at higher strain amplitudes, outside of the measuring range. For the NAC-PSAs maxima of S cannot be observed which might be a consequence of too small strain amplitudes. This detected intra-cycle strain stiffening behavior of S , for AC- and NAC-PSAs in varying levels, might be attributed to the stretching and yielding of the molecular network as reported by [51, 54, 55].

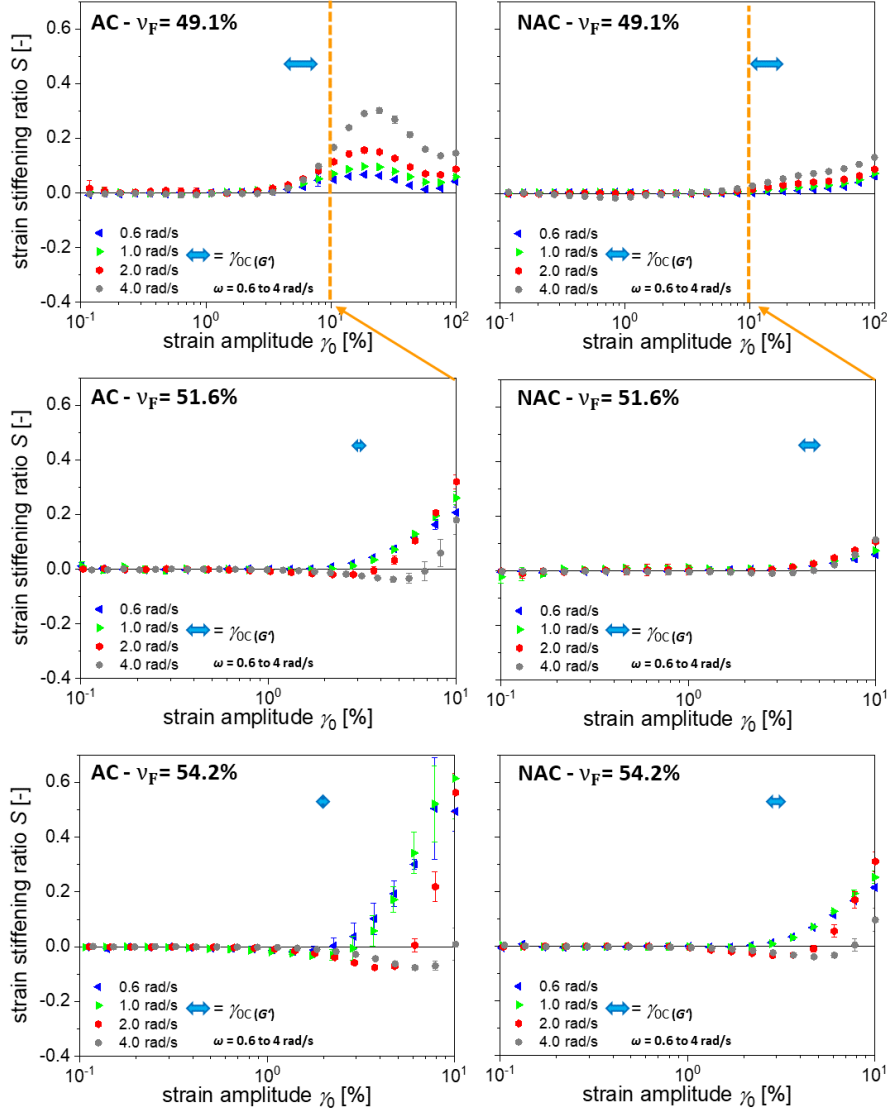


Fig. 11: Strain amplitude and frequency dependent strain stiffening ratios S for AC- and NAC-PSAs [36].

Fig. 12 shows the viscous nonlinear behavior with the shear thickening T ratio, displaying a v_F and frequency dependency for both, AC- and NAC-PSAs. AC-PSAs with $v_F = 49.1\%$ display an intra-cycle transition from shear thickening ($T > 0$) at moderate strain amplitudes to intra-cycle shear thinning ($T < 0$) at higher strain amplitudes. Whereas both PSAs with $v_F > 51.6\%$ display a strongly frequency dependent intra-cycle transition from shear thickening to shear

thinning. As the shear thickening maxima are shifted to lower strain amplitudes with increasing v_F and decreasing frequencies, one may assume that the shear thickening behavior occurs initially before a shear thinning behavior is attained at higher strain amplitudes, similar to the PSAs with $v_F = 49.1\%$. Various researchers [49, 50, 53, 54] reported similar findings with increasing polymer concentrations / filler contents and explained these findings with the creation of a shear induced filler network or gelation due to particle-particle interactions or physical cross-links at moderate strain amplitudes. A further increase of the applied strain amplitude causes the orientation of the polymer chains or stretching of the network and may lead to the destruction of the shear induced network.

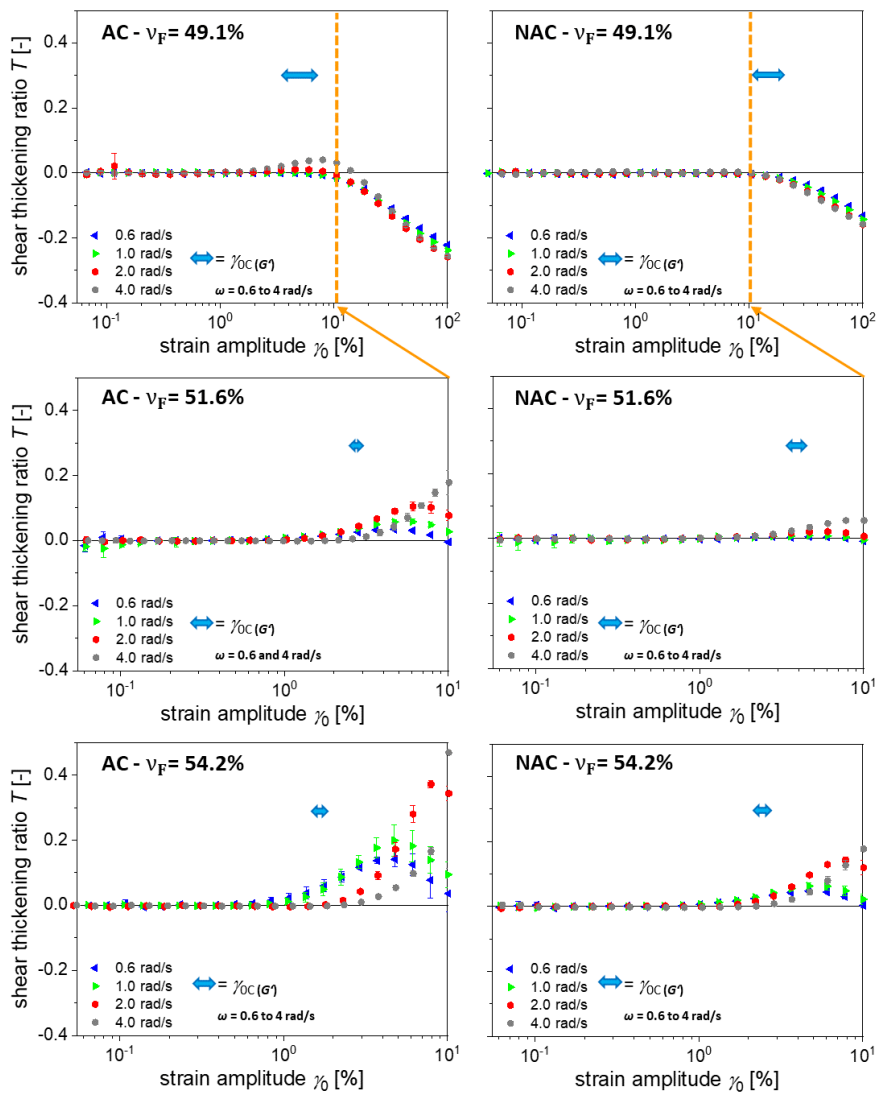


Fig. 12: Strain amplitude and frequency dependent shear thickening ratios T for AC- and NAC-PSAs [36].

4.2 Diffusion properties [37]

During the application of TTS on human skin, sweat and individual skin characteristics affect the adhesion of TTS to the skin. However, as evaporation of water molecules is prevented by an occlusive backing layer that covers TTS, water and sweat released from the skin possibly diffuses into the PSA and might affect the PSA's mechanical properties and its adhesion behavior. Therefore, the effect of diffusing molecules as deionized water and a 0.9 % NaCl solution into the PSA was investigated.

4.2.1 Diffusion into PSA monitored with DEA [37]

For monitoring the diffusion kinetics of deionized water and 0.9 % NaCl solution into silicone AC- and NAC-PSAs, the dielectric analysis (DEA) within a temperature controlled fringe field mini-IDEX sensor setup was used, **Fig. 13a-c**).

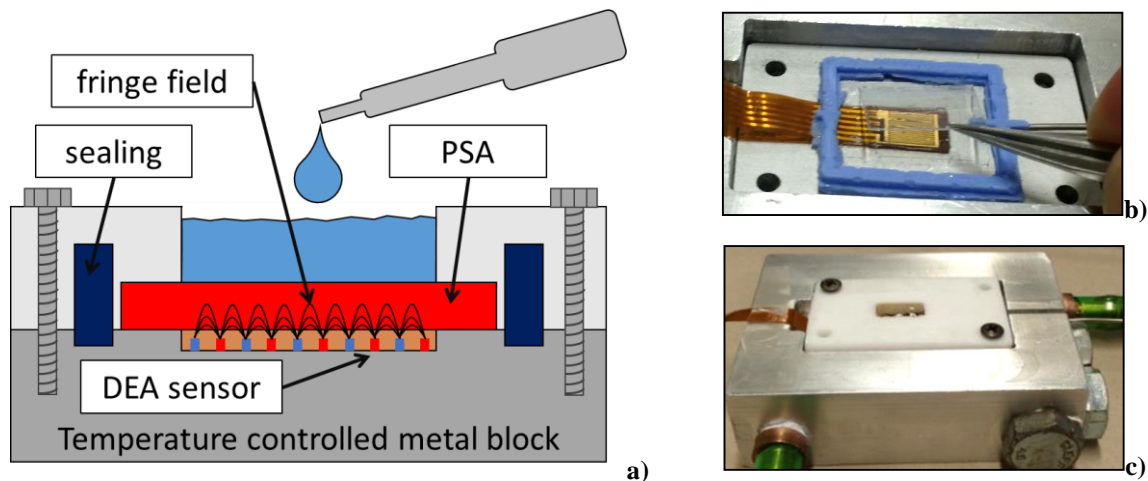


Fig. 13 a-c): Cross sectional sketch of the experimental setup with a temperature controlled metal block, sealing, the DEA mini IDEX-sensor, the fringe field of the DEA sensor, the PSA-film and the applied diffusant on the PSA-film a), stacked PSA-films are positioned on the mini-IDEX sensor, enclosed by the sealant b), water-temperature controlled aluminum-block with PTFE-covering plate, added onto the mini-IDEX sensor setup [37].

Fig. 14 shows a schematic time dependent DEA curve that monitors the diffusion process of deionized water into a silicone PSA, resulting in an η^{ion} -time curve. Before the addition of water, η^{ion} displays a stable signal until it decreases asymptotically shortly after the addition of water. From that η^{ion} -time curve, the following characteristic parameters can be extracted:

- constant initial ion viscosity η_0^{ion}
- final ion viscosity $\eta_{\infty}^{\text{ion}}$

- ion viscosity $\eta_{\tau_{25\%}}^{\text{ion}}$, 25 % below η_0^{ion}
- time $\tau_{25\%}$ at $\eta_{\tau_{25\%}}^{\text{ion}}$
- ion viscosity $\eta_{\tau_{63\%}}^{\text{ion}}$, 63 % below η_0^{ion} and
- time $\tau_{63\%}$ at $\eta_{\tau_{63\%}}^{\text{ion}}$.

Evaluation of the η^{ion} -time curves display decreasing η_0^{ion} and $\eta_{\infty}^{\text{ion}}$ with increasing thickness, at least partially, [37]. It can be assumed that constant values of η_0^{ion} and $\eta_{\infty}^{\text{ion}}$ prior and after diffusant addition and saturation, respectively, occur and depend only on materials investigated but not on sample thickness. Furthermore, the relatively large STD of the ion viscosities η_0^{ion} and $\eta_{\infty}^{\text{ion}}$ indicate possible inhomogeneity's that occur during the sample handling. Moreover, within the range of the experiment, η_0^{ion} and $\eta_{\infty}^{\text{ion}}$ do not show a v_F dependency, which might be attributed to the fact that all investigated PSA's are in the rubbery state with highly mobile polymers that a variation of $v_F = 5\%$ does not cause large effects.

The times $\tau_{25\%}$ and $\tau_{63\%}$ increase with increasing PSA thickness. Similar findings were reported by Wang and Asaoka [56, 57] for vulcanized silicone rubber and dental resin components. Moreover, the times $\tau_{25\%}$ and $\tau_{63\%}$ of NAC are about double of the times of AC, which can be explained by the polar $-\text{OH}$ end-groups within NAC-PSA leading to polar interactions with the diffusant and therefore restraining the diffusion rate. This restraining behavior of the diffusant does not occur for AC-PSA with its $-\text{CH}_3$ end-groups. Furthermore, the times $\tau_{25\%}$ and $\tau_{63\%}$ do not show great differences, with respect to the STD, between deionized water and 0.9 % NaCl solution, due to the low concentration of NaCl ions.

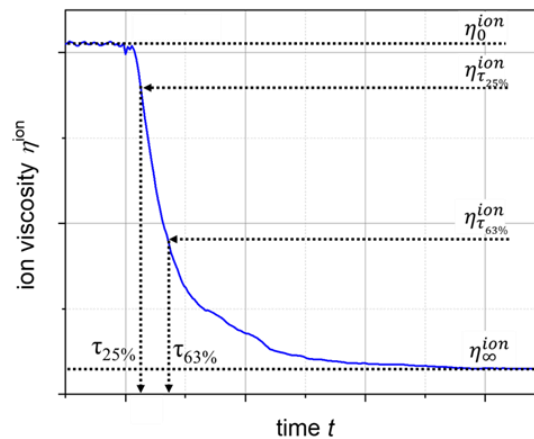


Fig. 14: Time dependent η^{ion} -time curve from the DEA to monitor the process of diffusing water into a silicone PSA, with characteristic evaluated points [37].

Thermal coefficient of expansion (CTE) before and after T_g was determined by DMA, to calculate T -dependent relative free volume v_{free} for evaluation of η^{ion} -

time curves and the diffusion coefficients. The results from DMA measurements displayed a T_g at the maximum of $\tan(\delta)$ at -120 °C, being independent of the PSA's v_F [37]. The CTE in the glassy state, approx. $450 * 10^{-6}/K$, increased with decreasing v_F and are half of the CTE in the liquid state, approx. $900 * 10^{-6}/K$, which do not show a v_F dependency, from which a v_{free} of around 10 % can be calculated, [37]. Furthermore, for diffusion coefficient evaluation, water uptake m_∞ of the PSAs had to be determined. The results showed that the AC- and NAC-PSAs absorbed hardly any water but the polar $-OH$ groups of NAC cause a clearly higher water uptake than the nonpolar $-CH_3$ groups of AC [37]. Furthermore, m_∞ displays for deionized water increasing values with decreasing v_F for AC- and NAC-PSAs due to decreasing v_F and subsequently increasing v_{free} . On the contrary, uptake of 0.9 % NaCl decreases with decreasing v_F for AC-PSAs while results remain constant for NAC-PSAs.

Based on the small amounts of water uptake, it can be assumed that the water diffuses rather as vapor within the free volume of the PSA. Therefore, the following equation can be evolved by combining the equations of Crank [22], Zahouily et al., Fieldson, Lee, Zeghbreek, and Doolittle [58-62] for describing the diffusion process for sample thicknesses ($d_{max} > d_{PSA}$), monitored with the DEA:

$$lg\eta^{ion}(t, \omega) = A + B + \frac{\frac{B}{v_{free}}}{1 + \left\{ 1 - \frac{8}{\pi^2} \frac{d_{PSA}}{d_{max}} \sin\left(\frac{\pi d_{max}}{2 d_{PSA}}\right) \exp\left(\frac{-t}{\tau_{diff}}\right) \right\}} \quad \text{for } d_{max} > d_{PSA} \quad (15)$$

with the ion viscosity η^{ion} , the contribution of the final ion concentration to the ion viscosity A , the Doolittle material constant B , the free volume v_{free} , the thickness of the PSA d_{PSA} , the maximum range of the DEA d_{max} , the time t , and the diffusion time constant τ_{diff} . For the diffusion with ion transport, the initial ion concentration c_{ion}^0 , the constant k_2 , and the maximum diffusant concentration c_{∞}^{PSA} are unknown quantities and can be aggregated to the constant K_2 , resulting in:

$$lg\eta^{ion}(t, \omega) = A + B + \frac{\frac{B}{v_{free}}}{1 + \left\{ 1 - \frac{8}{\pi^2} \frac{d_{PSA}}{d_{max}} \sin\left(\frac{\pi d_{max}}{2 d_{PSA}}\right) \exp\left(\frac{-t}{\tau_{diff}}\right) \right\}} - lg \left(1 + K_2 \left\{ 1 - \frac{8}{\pi^2} \frac{d_{PSA}}{d_{max}} \sin\left(\frac{\pi d_{max}}{2 d_{PSA}}\right) \exp\left(\frac{-t}{\tau_{diff}}\right) \right\} \right), \text{ for } d_{max} < d_{PSA} \quad (16)$$

with K_2 as a measure of the maximum contribution of absorbed ions on $\eta^{ion}(t)$ on account of the diffusing ions.

The diffusion time constant τ_{diff} from eq. 15 and 16 allows for the determination of the diffusion coefficient D :

$$D = \frac{4d_{PSA}^2}{\pi^2\tau_{diff}} \quad (17)$$

Influence of chemical composition and PSA-film thickness on the diffusion behavior [37]

The normalized η^{ion} -time curves show the influence of the thickness and the chemical composition for the diffusion of distilled water into AC- and NAC-PSAs, **Fig. 15**. Both materials display increasing diffusion times until the final ion viscosity $\eta_{\infty}^{\text{ion}}$ is reached, which can be explained by the longer diffusion lengths which has to be passed by the diffusing water molecules. NAC- exhibits longer diffusion times than AC-PSAs. This can be attributed to the polar –OH end-groups within the NAC-PSA, causing a slowdown effect due to the established hydrogen bonds with the diffusing water molecules, whereas the AC-PSA features nonpolar hydrophobic –CH₃ end-groups which result in weaker van der Waals forces that delay the diffusing water molecules less than the –OH end-groups.

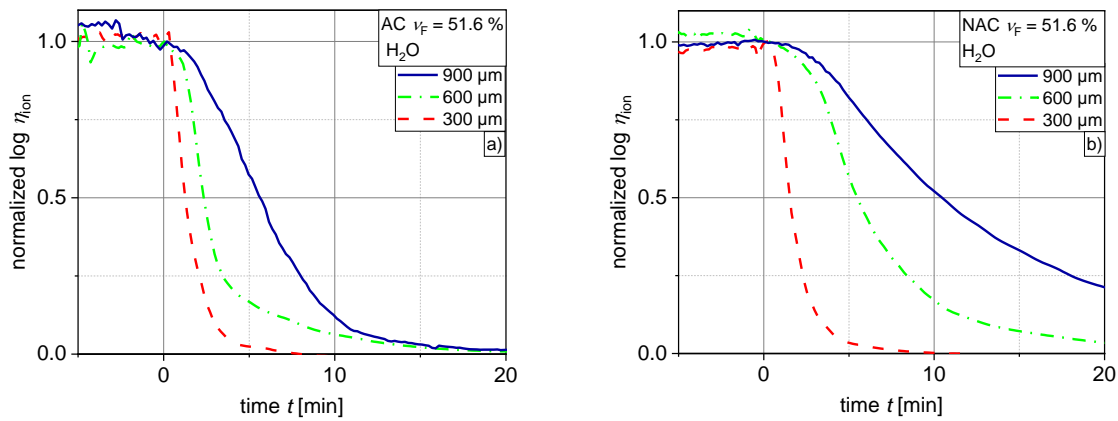


Fig. 15: Ion viscosity (η^{ion}) as a function of time (t) for various film thickness of a) AC and b) NAC PSA-films (resin content of $v_F = 51.6\%$) [37].

The diffusion coefficients D for AC- and NAC-PSAs were fitted with eq. 15 for deionized water and eq. 17 for 0.9 % NaCl solution. As eqs. 15 and 16 describe the diffusion process only for diffusion time constants $> \frac{\tau_{\text{diff}}}{2}$, starting times of 330 s, 1300 s and 3000 s were chosen for the thicknesses of 300 μm , 600 μm , and 900 μm , respectively. The diffusion coefficients D reveal no thickness dependency, with respect to STD, while D -values of NAC- are lower than those of AC-PSAs, reflecting the hindered and therefore slower diffusion within NAC-PSAs being caused by the formed hydrogen bonds with the –OH end groups, [37].

Influence of the resin content and PSA-film thickness on the diffusion behavior [37]

Both AC- and NAC-PSAs reveal a v_F dependent diffusion behavior for deionized water, **Fig. 16**. A decreasing v_F leads to higher D -values for AC-PSAs and shorter diffusion times until saturation at $\eta_{\infty}^{\text{ion}}$ is reached, [37]. The silicone PSAs are

composed of a polymer and a resin phase, where the first phase consists of linear polydimethylsiloxane (PDMS) molecules, while the second phase is a complex cross-linked network [6]. The cross-linked structure of the resin leads to small intra- and intermolecular distances and causes an inflexibility which results in low molecular motion. Therefore, an obstruction of the diffusing molecules within the resin can be expected. Whereas the linear PDMS molecules are able to rotate and move freely within its range of motion, easing pathways for the diffusing molecules. The increased range of motion results in a higher free Volume v_{free} with decreasing v_{F} and explains the improved diffusion of the water molecules within the non-polar AC-PSA with the lowest v_{F} .

Besides, NAC-PSAs displays a contrastive effect – smaller D -values and shorter diffusion times with increasing v_{F} until saturation at $\eta_{\infty}^{\text{ion}}$ is reached, [37]. This can be explained by an effect that is caused by the polar –OH end-groups. A lower v_{F} lead to increasing spatial gaps within the PSA, resulting in wider distances of the resin molecules and therefore to –OH end-groups that can easily interact with the diffusant and cause its obstruction. Whereas a higher v_{F} induce more compact spatial gaps in the PSA, thus leading to smaller distances of the resin molecules. This promotes the interaction of intermolecular –OH end-groups of the PSA, being blocked by their selves and thus being unavailable for the diffusing water molecules which can diffuse more easily.

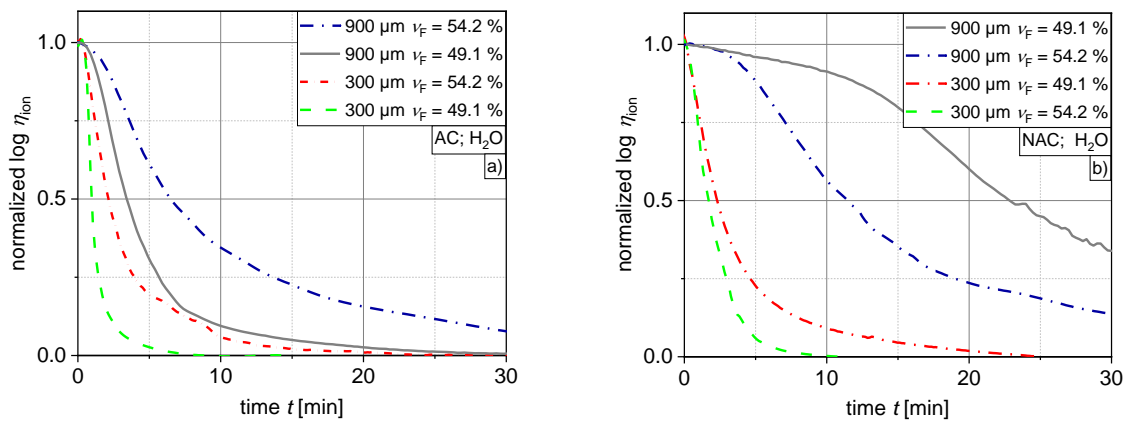


Fig. 16: Influence of v_{F} and the PSA-film thickness of AC a) NAC PSA-films b) [37].

Influence of the diffusant on the diffusion behavior [37]

The influence of the diffusant was investigated by using an isotonic 0.9 % NaCl solution for the diffusion measurements within the AC- and NAC-PSAs. The $\eta^{\text{ion}}-t$ curves were first evaluated by eq. 15 and subsequently by eq. 16 to quantify the effects of the diffusion ions. The results of eq. 15 showed that the diffusion times and the D -values increase for both PSAs, when a 0.9 % NaCl solution is used,

Fig. 17, [37]. This can be explained by the formed hydration shells around the Na^+ - and Cl^- - ions, which increase the size of the diffusing molecules and thus leads to a blocking of diffusion pathways. Furthermore, Millero et al. [63], Marcus [64], Hindman [65], Impey et al. [66], and Heyrovská [67] reported hydration numbers of 3.7, 3.2, 4 and 3.4 for Na^+ and 2, 2.6 and 2.5 for Cl^- , resulting in factor 3.9 and 2.2 higher masses for Na^+ and Cl^- , respectively, thus leading to a reduced diffusion velocity for these hydrated ions. Therefore, the diffusion of NaCl-solution is hindered, and thus slower in comparison to deionized water. [68, 69].

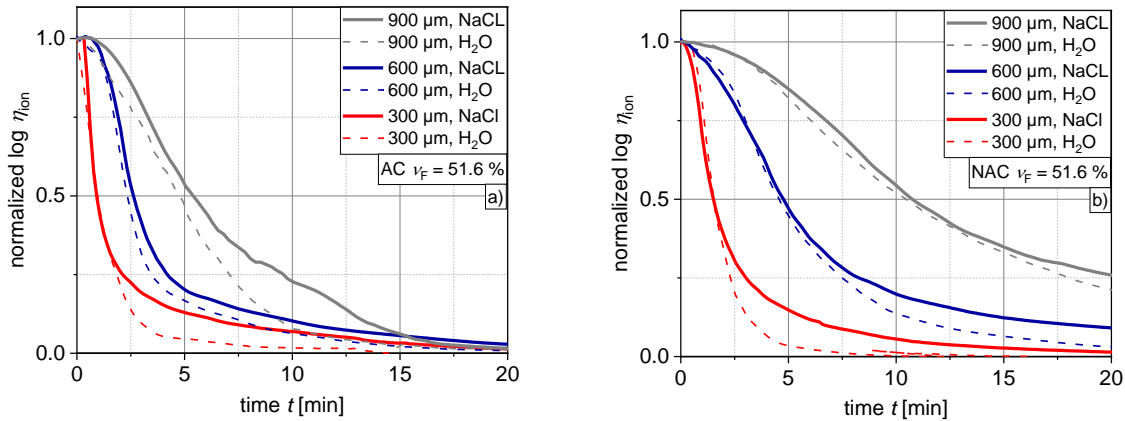


Fig. 17: Influence of diffusant and PSA-film thickness of AC a) NAC PSA-films b) [37].

The results of eq. 16, with K_2 as representative parameter attributing the effect of diffusing ions, displayed similar D -values from eq. 16 and very small K_2 -values [37]. Therefore, the diffusion of ions within AC- and NAC-PSAs is negligible.

Additionally, parameter A , eq. 16, contains sample thickness independent initial material properties such as rheological viscosity, ion concentration and ion charge. Moreover, the Doolittle constant B represents a thickness independent material constant. Therefore, a thickness averaging showed that parameter A decreases with decreasing v_F , whereas the Doolittle constant B and D increase with decreasing v_F , **Table 4**. Although the scatter of the STD for A and B are rather large, both parameters are constant for AC- and NAC-PSAs and show a v_F dependency and a differentiation with respect to the chemical composition.

Table 4: Resin content dependent thickness averages of parameter A , parameter B and diffusion coefficients D of AC- and NAC-PSAs [37].

property	AC			NAC		
	diffusant deionized water			diffusant deionized water		
resin content v_F	54.2 %	51.6 %	49.1 %	54.2 %	51.6 %	49.1 %
parameter A	7.0 ± 0.7	6.0 ± 0.7	5.4 ± 0.4	5.8 ± 0.7	5.2 ± 0.2	3.7 ± 1.3
Doolittle constant B	12.5 ± 2.5	24.0 ± 14.9	40.3 ± 20.1	3.3 ± 9.7	41.3 ± 16.4	59.7 ± 4.7
Diffusion coefficient D in 10^{-8} cm ² /s	145 ± 19	246 ± 5	332 ± 42	129 ± 9	185 ± 2	193 ± 4
	diffusant 0.9 % NaCl-solution			diffusant 0.9 % NaCl-solution		
resin content v_F	54.2 %	51.6 %	49.1 %	54.2 %	51.6 %	49.1 %
parameter A	6.4 ± 0.4	5.8 ± 1.5	5.3 ± 0.7	6.5 ± 0.1	5.7 ± 0.9	5.3 ± 0.8
Doolittle constant B	15.0 ± 3.3	17.3 ± 7.4	22.2 ± 10.7	12.8 ± 5.2	20.0 ± 5.9	34.0 ± 10.2
Diffusion coefficient D in 10^{-8} cm ² /s	111 ± 9	146 ± 31	232 ± 13	99 ± 4	113 ± 7	172 ± 17

The DEA allows for the investigation of the diffusion properties of deionized water and an isotonic NaCl solution into AC- and NAC-PSAs. The η^{ion} and the diffusion coefficients evaluation show a clear influence of the PSAs chemical composition, its resin content and the diffusant. Therefore, these results from this method lead to a better understanding of occurring diffusion mechanisms within the PSA and this knowledge can be used within further development of TTS.

4.3 Adhesion properties

In this thesis, the adhesion properties of silicone-based AC- and NAC-TTS were tested according to standardized testing procedures probe tack (ASTM D2979) [14], adhesion strength (DIN EN ISO 29862) [16] and with the developed testing approach– *RheoTack* [38]. To obtain a deeper insight into these adhesion properties, standard testing was compared with the newly developed approach.

4.3.1 Standardized tests – probe tack and shear strength

Probe tack measurements record only the maximum force during retraction of a stainless steel plate $\varnothing = 5$ mm from the TTS. Both TTS types show a decreasing probe tack with increasing v_F , **Fig. 18 a**). This can be explained by the fact that the resin serves as the crosslinking agent, resulting in a denser network [5, 6, 9]. From a higher cross-linking degree, a higher viscosity can be expected [36], leading to a reduced wettability of a surface. This can cause a reduced mechanical anchorage of the PSA, and therefore the tack forces decrease with increasing v_F .

Probe tack values of NAC-TTS exceed those of AC-TTS by a factor of 1.2-10.5 for $\nu_F = 49.1\%$ to $\nu_F = 54.2\%$, respectively. This could be a result of the end-group replacement from polar $-\text{OH}$ to non-polar $-\text{CH}_3$ groups, **Fig. 2**. As a result, a higher molecular weight and a possibly higher cross-linking degree for AC-TTS can be expected [36], leading to a reduced wettability and a lower tack force. Furthermore, these non-polar end-groups cannot create polar interaction with the metal surface of the rod, and therefore leads to the reduced adhesion.

The peel adhesion testing was performed in 180° angle by retracting a TTS from stainless steel plates with 300 mm/s. **Fig. 18 b)** shows the mean force of 50 mm retraction distance, quantifying TTS removal from the metal substrate. In contrast to the probe tack results, the peel adhesion forces increase with increasing ν_F , which can be explained by the increasing crosslinking density causing a higher cohesiveness of the PSA. Although AC-TTS exhibit nonpolar $-\text{CH}_3$ end-groups, the possibly higher crosslinking density causes 1.02 to 1.2 times higher values of the peel force than those of NAC-TTS.

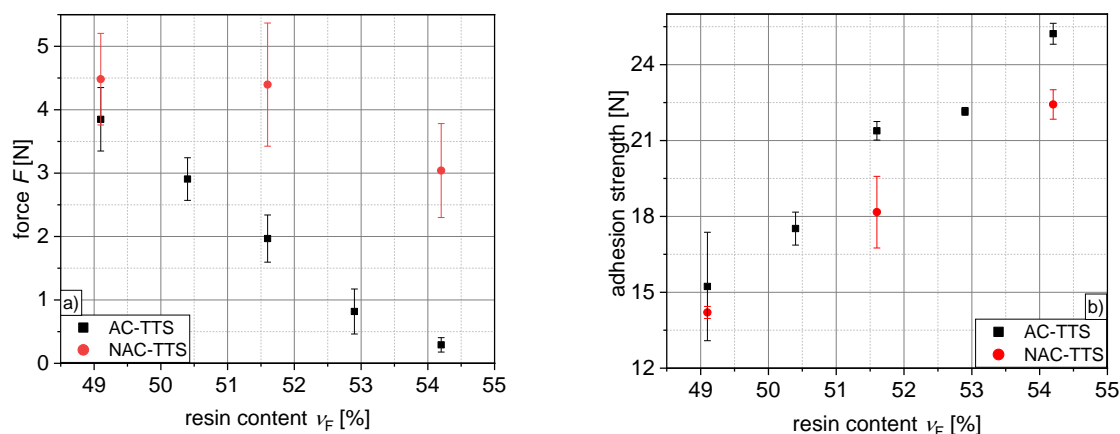


Fig. 18: Resin content dependent results from probe tack a) and peel adhesion strength testing for AC- and NAC-TTS.

4.3.2 RheoTack development [38]

The *RheoTack* approach was developed by using the rheometer's normal force sensor to characterize the adhesion and detaching properties and detaching mechanisms of patches. A plate and plate geometry of a rotational rheometer) was used to determine the tack behavior of adhesive patches combined with a video monitoring system to record occurring PSA deformations. The new approach includes a sample holding ring as an exchangeable temperature module plate (TMP), an optical observation unit consisting of three cameras for synchronized video monitoring, an illumination unit, and exchangeable probe rod geometries, **Fig. 19**.

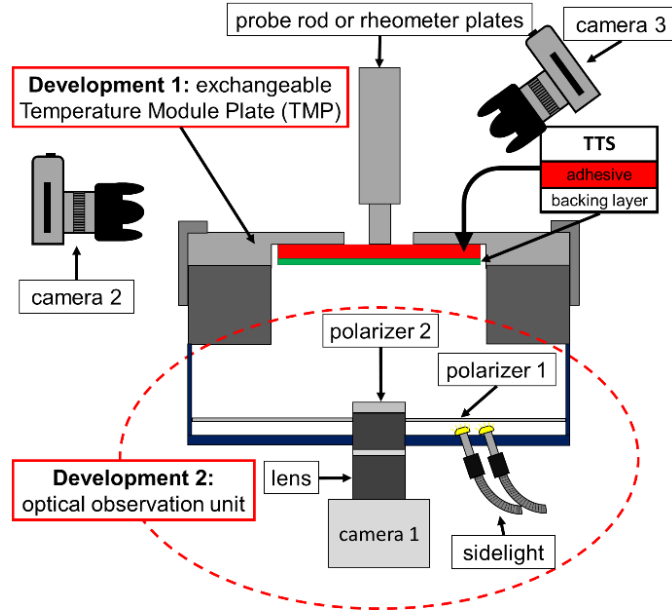


Fig. 19: Sketch of the *RheoTack* approach with the upper plate as the probe rod, the temperature module plate (TMP) for patch fixation as the lower plate, and the implemented optical observation unit for synchronized video monitoring from the bottom (90 °, camera 1), lateral (0°, camera 2), and top (45°, camera 3) to the rheometer [38].

4.3.3 RheoTack data evaluation and results [38]

The *RheoTack* approach provides a force-retraction displacement ($F-h$) curve with synchronized visual information from video monitoring. Compared to the standardized probe tack test as a single point measurement [14], the *RheoTack* $F-h$ curve contains significantly more information, with the compression, stretching and fibrillation, and the detaching phase. Furthermore, *RheoTack* quantities can be determined from the $F-h$ curve, **Fig. 20**:

- the slope of the $F-h$ curve at $h = 0$ represents the sample stiffness S ,
- the initiation force of cavity or fibril formation $F_{\text{start fib}}$ and the corresponding displacement $h_{\text{start fib}}$ can be determined,
- the area under the $F-h$ curve until $F_{\text{start fib}}$ serves as the activation energy of cavity and/or fibril formation $E_{\text{start fib}}$,
- maximum force F_{max} and corresponding displacement h_{max} equals the maximum load capacity of the adhesion system,
- the integral of the entire $F-h$ curve corresponds to the adhesion energy E_{adh} and is a measure for the energy of the complete detaching process.

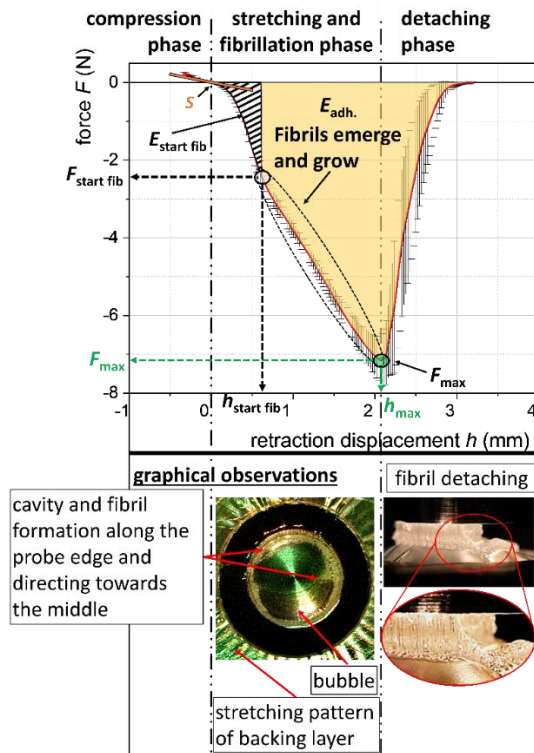


Fig. 20: Evaluation of $F-h$ curve with deformation phases and characteristic *RheoTack* quantities: S , $F_{\text{start fib}}$, $h_{\text{start fib}}$, $E_{\text{start fib}}$, F_{max} , h_{max} , E_{adh} and corresponding structures[38].

The influence of v_{retract} , v_F , PSA-type (AC, NAC), and probe rod geometry was investigated by evaluating the *RheoTack* quantities [38, 39].

Influence of the retraction speed v_{retract} [38, 39]

Fig. 21 shows the influence of v_{retract} on NAC-TTS with $v_F = 49.1\%$ and displays that an increasing v_{retract} causes higher negative forces at the same retraction displacement which is a clear demonstration of the viscoelastic behavior. Additionally, this is also shown by increasing stiffness, decreasing retraction displacements, $h_{\text{start fib}}$, h_{max} , and decreasing adhesion energies $E_{\text{start fib}}$, E_{adh} , [39].

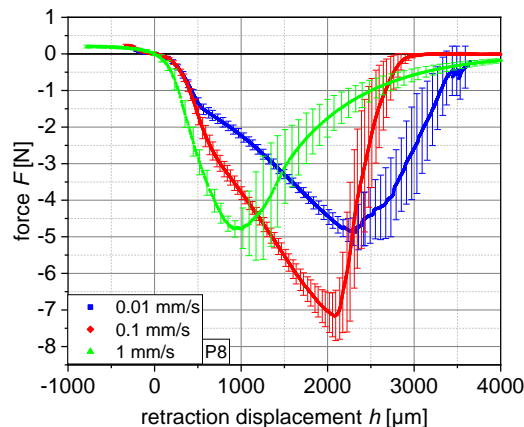


Fig. 21: Mean force $F-h$ curves from *RheoTack* testing at retraction speeds of 0.01, 0.1 and 1 mm/s obtained for five different TTS samples (NAC-TTS 49.1 %) [38].

Furthermore, it was found that an increasing v_{retract} leads to shorter compression phases, [37], less time for the PSA to wet the probes surface, less mechanical anchorage, and therefore to lower tack values.

Table 5: Retraction speed dependent compression times [39].

Retraction speed [mm/s]	Compression time [s]		
	P8	P5	R5
0.01	27.7	27.9	31.6
0.1	6.0	7.0	9.1
1	3.1	3.3	3.5

Influence of the PSA's resin content v_F [39]

An increasing amount of resin content v_F leads to decreasing force values, retraction displacements and adhesion energies, **Fig. 22**. As the resin serves as a crosslinking agent in the PSA, it causes a network creation and leads to a “bodied” silicone PSA [5, 6, 9]. Thus, with an increasing v_F , an increasing crosslinking density within the PSA can be expected and causes a stiffer material behavior. Furthermore, a higher cross-linking density leads to a higher viscosity and reduced wettability of a surface, resulting in a reduced mechanical anchorage. Therefore, the tack forces decrease with increasing v_F , [39]. Moreover, a higher v_F causes a decreased stretchability of the PSA that results in decreased retraction displacements and correlates with the increase of the cross-linking density.

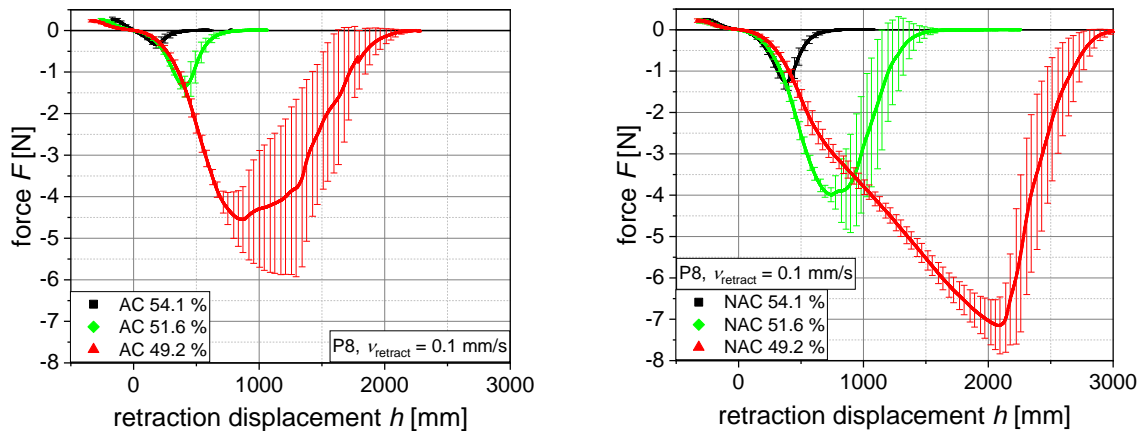


Fig. 22: F - h curves of AC- and NAC-TTS with $v_F = 54.2 \%$, 51.6% and 49.1% , tested with retraction speed of $v_{\text{retract}} = 0.1 \text{ mm/s}$ with P8 [39].

Influence of the PSA type (AC, NAC) [39]




For the same v_F , NAC-TTS displays lower stiffness S , higher tack force values, retraction displacements, and adhesion energies than AC-TTS, [39]. This result can be explained by two effects. First, the polar OH-end groups of the NAC-TTS

establish more polar interactions with the metal substrates compared to the CH₃-end groups, leading to a better adhesion and higher adhesion energies for the NAC-TTS. Second, the 2nd polycondensation step for the end-group replacement from –OH (NAC) to –CH₃ (AC) might affect the crosslinking density and therefore the viscosity, wettability, mechanical anchorage, stretchability, and tack force. As a consequence, the higher cross-linking density of AC would lead to a higher viscosity, which can be confirmed by rheological measurements, [36, 39].

Influence of the probe rod geometry and evaluation from the optical observations [38, 39]

As the *RheoTack* approach allows for the installation of different rods, the following probe rods were used within the performed experiments, **Table 6**:

Table 6: Rod geometries used with their dimensions and surface roughness's [39].

Abbreviation	P8	P5	R5
Rod geometry	 Flat cylinder, large $A_{\text{contact}} \cong 50 \text{ mm}^2$	 Flat cylinder, small $A_{\text{contact}} \cong 20 \text{ mm}^2$	 Spherically rounded rod $D_{\text{sphere}} = 12 \text{ mm}$ $A_{\text{contact}} \approx 5 \text{ to } 10 \text{ mm}^2$
Diameter [mm]	8	5	5
Surface roughness Ra [μm]	0.43 ± 0.11	0.75 ± 0.41	0.24 ± 0.03

The rods reveal surface roughness's between 0.24 to 0.43 μm . However, the surface roughness of the three rods allow for comparison between the measurements, due to Chiche et al. findings [70]. Similar to the probe tack testing, an initial compression force of $F = 0.2 \text{ N}$ for all rods was used for the *RheoTack* measurements, which is achieved when the rod pushes the flexible TTS, adhering to the TMP's bottom, downward, **Fig. 23**. This leads for the different rods to contact pressures of 4 kPa (P8), 10 kPa (P5), and 64 kPa (R5) due to decreasing contact diameters from P8 (8 mm) to P5 (5 mm) and R5 (2 mm).

Moreover, the decreasing contact diameters lead to increasing inclination angles of the TTS in the gap from R5 to P5 and P8. The flexible backing layer of the TTS causes an inhomogeneous stress field within the TTS for all rods. While at the flat rods the stresses increase from zero in the center to the highest value at the circumferential stripe, at the spherical rod the highest stresses occur in the center,

which decreases to the outer ring where the TTS coincides with the tangent of the rod sphere. Hence, at the end of the dwell time, the retraction starts from the different tack and adhesion states with varying displacements, depending on the rod and also on the mechanical properties of the TTS, **Fig. 23**, [39] However, larger displacements during compression result in longer compression times, thus giving the PSA more time for establishing adhesion towards the rods.

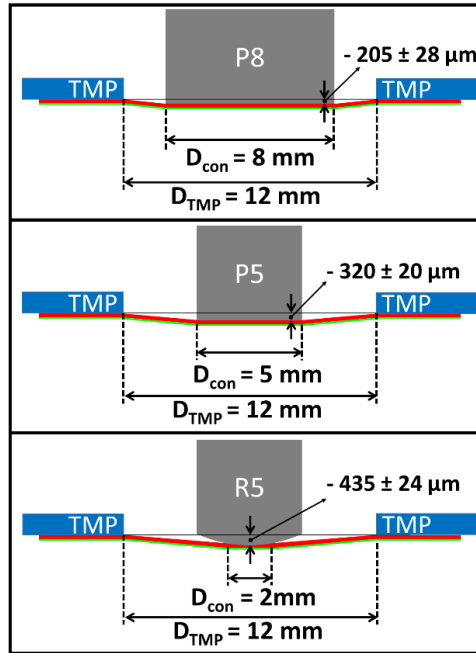


Fig. 23: Starting situation of the rods P8, P5 and R5 with the corresponding displacement and inclination angles at the end of the dwell time for NAC-TTS, $\nu_F = 49.1\%$ [39]

The *RheoTack* measurements showed, [39], that the chosen rod geometries affect the retraction speed dependent $F-h$ -curves significantly. The shapes of the $F-h$ -curves from the flat rods P8 and P5 are qualitatively similar, while the shape of the $F-h$ -curves from the spherical rod R5 differs significantly due to the different stress fields below the rods. This results in a one-force-maximum for the flat rods, while for R5 a plateau or a second-force-maximum after F_{\max} can be detected. Furthermore, it was found that tack quantities could not be determined for the stiffer TTS at higher retraction speeds. Especially with P8 and P5 the tack cannot be determined on AC- and NAC-TTS with higher ν_F , whereas R5 is able to measure the tack for all testing parameters. This is a consequence of the increasing contact pressures from P8 to P5 and R5. Therefore, the tack can be measured with R5 of TTS with the highest ν_F and ν_{retract} . For TTS with lower ν_F , P8 exhibits the highest *RheoTack* quantities due to the largest contact diameter, and therefore the largest adhesion surface (although it applies the lowest contact pressure).

For an independent comparison of the various rods, the measured forces of P8 and R5 were normalized on the basis on their contact area to the contact area of P5. Results in **Fig. 24** show normalized F - h -curves of AC- and NAC-TTS with $v_F = 49.1\%$. It is clearly visible that F_{\max} of P8 and P5 are in the same magnitude, whereas F_{\max} of R5 is larger for all v_{retract} . Furthermore, with R5 the force in the stretching and fibrillation phase increases significantly faster than with the flat rods. The comparison of the stretching and fibrillation phase of P8 and P5 displays that the retraction displacement after the kink point is larger for P8, showing that the fibril creation and elongation occurs over a longer period of time than for P5. This might be an effect of the larger contact and the resulting higher mechanical anchorage between the adhesive and the rod for P8.

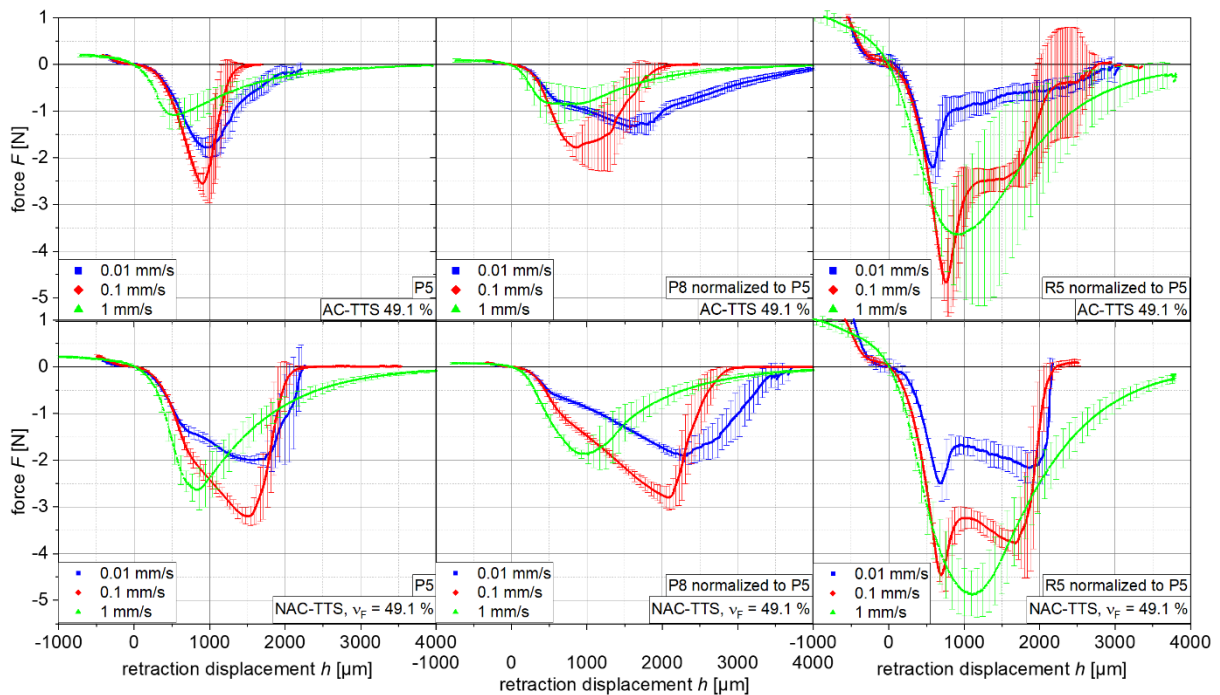


Fig. 24: Normalized F - h -curves (to P5) of P8, P5 and R5 for AC- (top) and NAC-TTS (bottom) with $v_F = 49.1\%$ [39].

During retraction, the inclined TTS in the gap forwards peel stresses to the rods, where the strength of the PSA is exceeded and causing the start of the failure at the contact line that propagates towards the interior of the PSA. Creton and Cicotti [71] stated that failure of a PSA consists of several steps, which start with nano-scaled cavitations. These cavitations dissipate deformation energy by large curvatures and stress concentration factors when the peel stresses of the PSA is exceeded. With further retraction the PSA has two options:

- crack propagation occurs perpendicular to the external load and causes catastrophic cohesive failure, or

- cavitations are lengthened and cause the reduction of local stress concentrations which leads to the start of fibril formation.

As described above, with P8 and P5 both failure options were observed. Especially TTS with higher ν_F at the highest ν_{retract} display the first option. From the synchronized optical observation at P8 and P5, it can be seen that the fibrils are created at the circumferential stripe of the rods. From here, the fibrils contract into the probe's middle, and cause simultaneous partial debonding that reduces the contact area of about 20 to 30 %, **Fig. 25**. A further retraction results in elongation, thinning and strain hardening of the fibrils at the rods circumference, until the first fibrils start to break at F_{max} . Thus, the resin content dependent moduli and retraction speed dependent parameter F_{max} displays a measure for fibril strength, fibril orientation, PSA flowability, stress relaxation, disentangling, and the strain-hardening process [72-74].

Furthermore, for both flat rods the optical observation showed that the retraction causes stretching patterns of the TTS and its withdrawal from the TMP's bottom from the initial edge of TTS $R_{\text{TTS},0}$ to the resulting TTS edge R_{TTS} , displaying that the PSA's shear strength is exceeded, **Fig. 25**.

Contrary to P8 and P5, for R5 only the fibril forming second option can be observed. As the contact area for R5 is in the range of only 2 to 2.5 mm, the transferred forces are relatively little and below the PSAs shear strength. Therefore, no visible stretching patterns and withdrawal of the TTS from the TMPs bottom can be observed, **Fig. 25**. At F_{max} the first fibrils break at the circumference. With ongoing retraction, the inner remaining fibrils are further elongated while the detaching moves in an orderly manner to the center of the rod. This process explains the moderate force decrease for AC-TTS after F_{max} , while for NAC-TTS a second maximum is observed. This can be explained by a higher strain hardening of the fibrils due to the higher interactions of the polymer chains among each other being caused by the polar OH- end-groups.

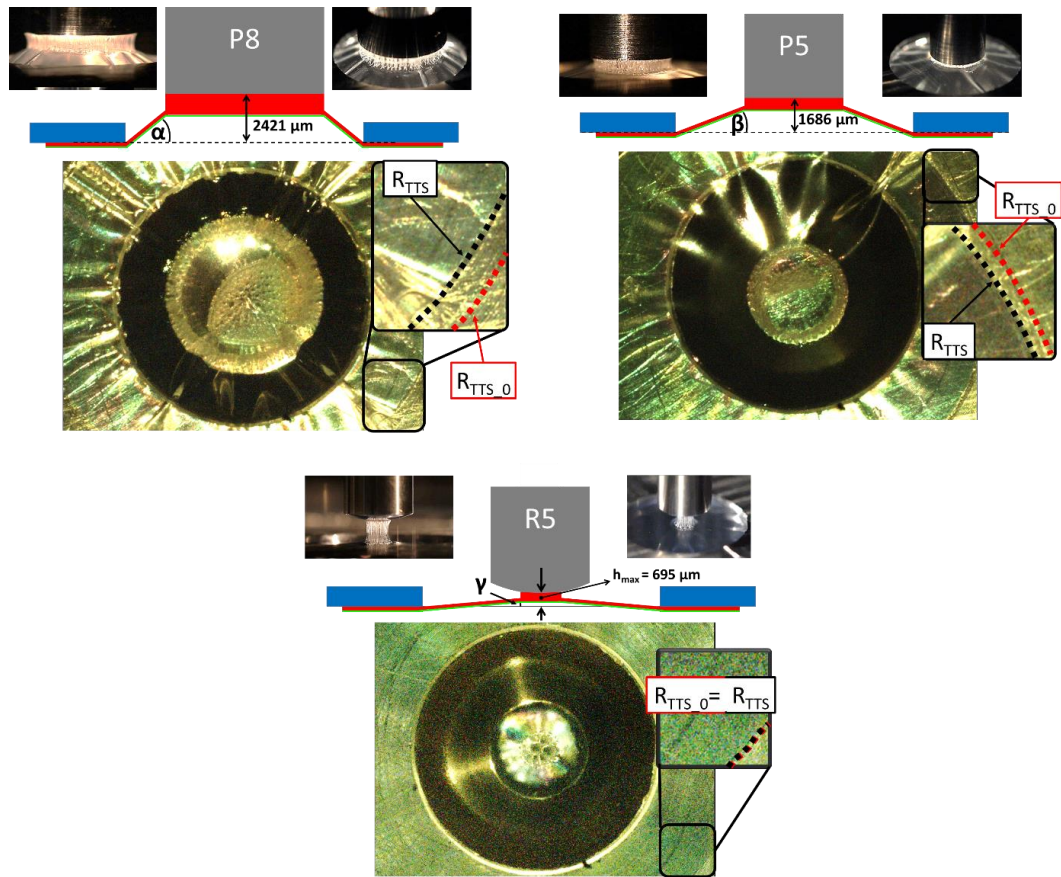


Fig. 25: State of bonding for P8 a), P5 b), and R5 c) at h_{\max} (NAC-TTS, $v_F = 49.1\%$ and $v_{\text{retract}} = 0.01\text{ mm/s}$) with stretching patterns of the backing layer between the TMP and rods, the resulting angles of the TTS between TMP and rods: α for P8, β for P5 and γ for R5, and the TTS's retraction at the TMPs bottom from initial edge of TTS $R_{\text{TTS},0}$ to the resulting edge of TTS R_{TTS} [39].

Additionally, further *RheoTack* evaluation displays the viscoelastic material behavior with increasing v_{retract} , which can also be seen by the optical observations, **Fig. 26**. These pictures show a higher v_{retract} leads to a reduced stretchability, shorter fibrils and results in a higher number of cavities, which decrease in size.

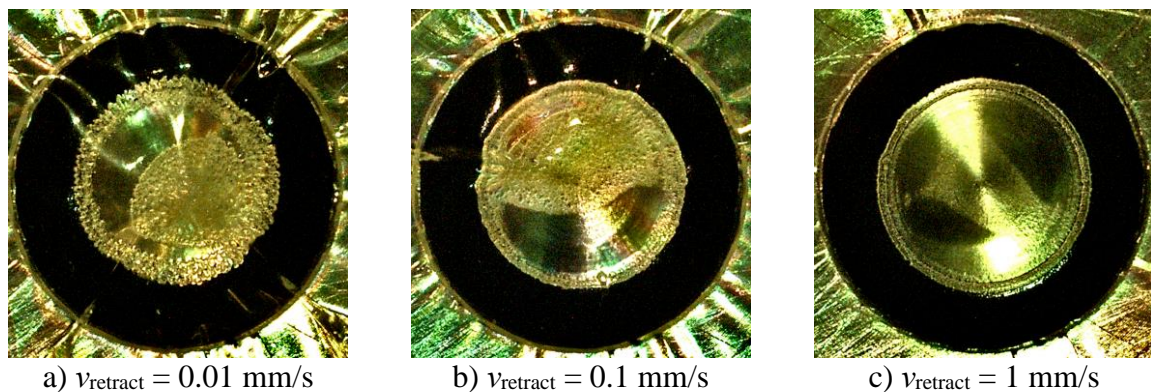


Fig. 26: Deformation structures as the stretching patterns of the TTS and cavity sizes observed with camera 1 under the probe rod in 90° , a) $v_{\text{retract}} = 0.01\text{ mm/s}$, b) $v_{\text{retract}} = 0.1\text{ mm/s}$, c) $v_{\text{retract}} = 1\text{ mm/s}$ [39].

RheoTack with its optical observation presents a powerful testing tool for the tack characterization of TTS and other backing layer supported patches. The resin content, the retraction rate and the rod geometry clearly influence the *RheoTack* results. Thus *RheoTack*, compared to standardized testing procedures, provides more essential information about viscoelastic properties, the adhesion and release behavior of TTS and allows for utilization within TTS development and quality assurance.

5 CONCLUSION

In this doctoral thesis, pressure sensitive adhesives (PSA) and transdermal therapeutic systems (TTS) were tested with traditional and newly developed application-related methods. This includes the investigation of the PSA within large amplitude oscillatory shear measurements to correlate the materials behavior during the patient's motion. The dielectric measurements show the effect of diffusing water into the PSA and allows for the determination of the diffusion coefficient. The development of the *RheoTack* approach displayed a comprehensive characterization of the TTS's adhesion and release behavior.

From the amplitude sweeps and Carreau-Yasuda-like modelling it can be concluded that all PSAs are located close to the gel point and their moduli increase with increasing resin content. From the nonlinear interpretation it can be concluded that a consolidation of the gelled network occurs, which is stretched and released by increasing strain amplitudes. The evaluation of the elastic and viscous Lissajous-Bowditch diagrams reveal that an increasing resin content causes an increasing shear thickening and strain stiffening effect, indicating an increasing yielding and stretching of the PSAs microstructure.

The monitored diffusion properties of water and an isotonic NaCl-solution into the PSA by dielectric analysis, were dependent in the PSA's chemical composition, the resin content, and the size of the diffusing molecule. The DEA diffusion setup gives a deeper insight into the diffusion mechanisms within the PSA and allows for the determination of the diffusion coefficient, and the investigation of the influence of released sweat and water of the patient.

The developed *RheoTack* approach with its optical observation unit revealed the role of TTS and PSA-composition, and testing conditions on the tack behavior. The PSA type and the resin content affect its flowability, mechanical anchorage and the resulting tack behavior and stretchability. Whereas the variation of the rod's retraction speed represents the PSA's viscoelastic material behavior and the rod geometry influences the detaching behavior. Testing of various TTS with the *RheoTack* approach showed that a low resin content with lower retraction speed causes high tackiness with stretched fibrils, while a high resin content and high retraction speed leads to non-adhesion and catastrophic failure of the TTS.

The thesis presents the newly developed and optimized application-related testing methods for an advanced product-oriented material testing, which allows for a significantly more reliable PSA and TTS characterization that can be utilized within further TTS development.

6 CONTRIBUTION TO SCIENCE AND PRACTICE

Transdermal therapeutic systems (TTS) are modern patch medication systems which allow facilitated treatment of various diseases by improving the patient's compliance e.g. displacing pill intake and reducing gastric load. Although TTS are available on the market since the 80th's, patients still report about poor adhesion properties causing an incorrect medication or even a complete failure of the patch, and thus of the therapy. As TTS development and quality assurance tests are still based on testing methods originating from technical bonding purposes, adhesion and therapeutic improvements are limited.

As TTS consist of a drug containing pressure sensitive adhesive and a protective backing layer subjected to both small and large deformations during application, testing methods have to be improved in terms of considering the patient's motion, the influence of released water and sweat during the application and the evaluation of the TTS's entire adhesion and release behavior. This requires knowledge about pressure sensitive adhesives (PSAs) and their adhesion-molecule-structure-property relationship.

This doctoral thesis is focused on the development of new TTS application-related testing methods and the characterization according to them. A PSA composition dependent study of TTS adhesion and release behavior with correlated small and large amplitude shear investigations were performed. Additionally, the diffusion property analysis of liquid molecules into PSAs was investigated. The following outcomes of this doctoral thesis are considered as the most important contributions to both, science and practice, **Fig. 27**:

- 1) The PSAs large amplitude oscillatory shear testing allows for advanced material characterization within large deformations, which can be used to interpret the PSAs behavior at skin motion during the TTS's application.
- 2) The dielectric analysis of diffusing water and an isotonic NaCl solution within the PSA allows for a comprehensive characterization of the diffusion process and the determination of the diffusion coefficient. Knowledge acquainted with testing method provides a better insight into the diffusion mechanisms within the PSA, and represents an application related testing for further TTS development.
- 3) *RheoTack* approach provides reliable insight into the retraction rate dependent adhesion and release behavior of TTS. The determination of seven *RheoTack* parameters and recorded pictures being correlated with the force-retraction displacement curve during the adhesion and detaching

process results in a significantly improved characterization of adhesion when compared to the standardized testing methods. Additionally, this knowledge can be used for the development and production of optimized TTS leading to a reduced therapy failure.

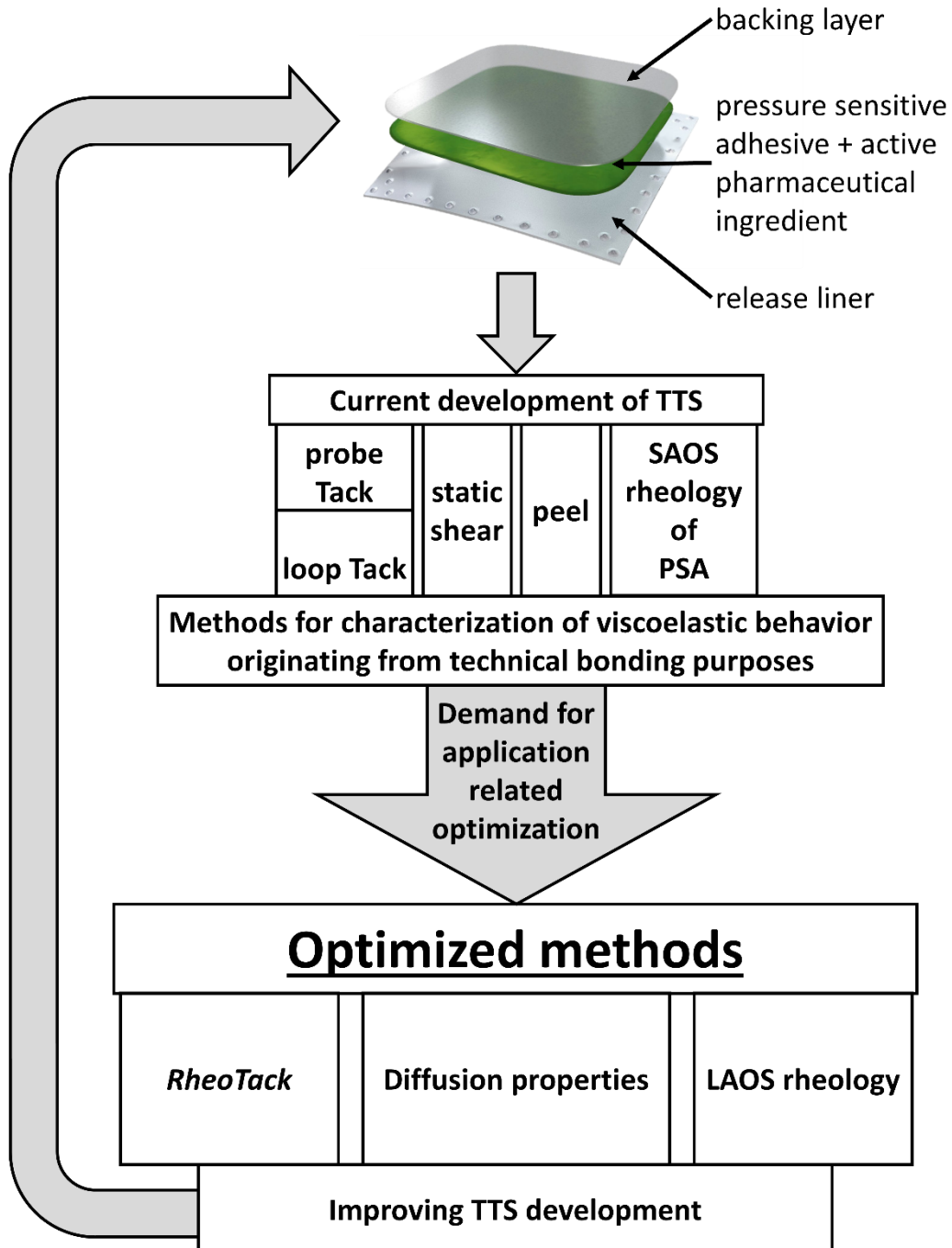


Fig. 27: Flow chart of the contribution to science and practice employed in the PhD. thesis [10].

REFERENCES

[1]	M. N. Pastore, Y. N. Kalia, M. Horstmann, M.S. Roberts, Transdermal patches: history development and pharmacology, <i>Brit. J. Pharmacol.</i> 172 (2015), 2179-2209.
[2]	U.S. Department of Health and Human Services Food and Drug Administration, Transdermal and Topical Delivery Systems- Product Development and Quality Considerations – Guidance for Industry (2019) https://www.fda.gov last accessed 27 th November 2023.
[3]	L. Webster, Recent developments in pressure-sensitive adhesives for medical applications, <i>Int. J. Adhes. Adhes.</i> 17 (1997) 69-73.
[4]	P. Minghetti, F. Cilurzo, A. Casiraghi, Measuring Adhesive Performance in Transdermal Delivery Systems, <i>Am. J. Drug Deliv.</i> 2 (2004) 193-206.
[5]	G.K. Schalau II, A. Bobenrieth, R. O. Huber, L. S. Nartker, X. Thomas, Silicone Adhesives in Medical Applications, in: <i>Applied Adhesive bonding on Science and Technology</i> , 2018, Intech Open, London, DOI: 10.5772/intechopen.71817 .
[6]	I. Benedek, M. M. Feldstein, Silicone Pressure-Sensitive Adhesives, in: <i>Technology of Pressure-Sensitive Adhesives and Products</i> , 2009, CRC Press Taylor&Francis Group, Boca Raton, ISBN: 978-1-4200-5939-7.
[7]	L. Mestach, S. Huygens, A. Goossens, L. Gilissen, Allergic Contact Dermatitis caused by Acrylic-bases Medical Dressings and Adhesives, <i>Contact Dermatitis</i> 79 (2018) 81-84.
[8]	A. Kunst, Thermodynamic Activity in PSA Matrices: Determination and influence on Skin Permeation, <i>Dissertation</i> , 2015, Friedrich-Alexander-Universität Erlangen-Nürnberg.
[9]	https://www.dupont.com , Review of silicone adhesives in healthcare applications, last accessed 27 th November 2023.
[10]	https://www.itslohmann.com , last accessed 27 th November 2023.
[11]	European Medicines Agency, Guideline on Quality of Transdermal Patches (2015) https://www.ema.europa.eu , last accessed 27 th November 2023.
[12]	International Council on Harmonisation of Technical Requirements for Registration of Pharmaceuticals for Human Use, Pharmaceutical Development Q8(R2) (2009) https://www.ema.europa.eu , last accessed 27 th November 2023.
[13]	International Council on Harmonisation of Technical Requirements for Registration of Pharmaceuticals for Human Use, Validation of Analytical Procedures: Text and Methodology Q2(R1) (2005) https://www.ema.europa.eu , last accessed 27 th November 2023.
[14]	American Society for Testing and Materials (ASTM), Standard Test Method for Pressure-Sensitive Tack of Adhesive Using an Inverted Probe Machine – ASTM D 2979 Vol. 15-10, 2016, ASTM International West Conshohocken.
[15]	CEN European Committee for Standardization, Adhesives for paper and board, packaging and disposable sanitary products – Tack measurement for pressure sensitive adhesives – Determination of loop tack – DIN EN 1719:1998, 1998, Beuth Verlag GmbH, Berlin.

[16]	CEN European Committee for Standardization, Self-adhesive tapes - Determination of peel adhesion properties ISO 29862:2018, 2019, Beuth Verlag GmbH, Berlin.
[17]	CEN European Committee for Standardization, Self-adhesive tapes - Measurement of static shear adhesion ISO 29863:2018, 2019, Beuth Verlag GmbH, Berlin.
[18]	German Institute for Standardization e.V., Rheometry- Measurement of rheological properties using rotational rheometers - Part 4: Oscillatory rheology – DIN 53019-4, 2016, Beuth Verlag GmbH, Berlin.
[19]	L. H. Sperling, Introduction to physical polymer science, 4th edition, 2006, Wiley, New Jersey, ISBN: 13 978-0-471-70606-9.
[20]	M. Michaelis, Characterization of Pressure Sensitive Adhesive Systems for Transdermal Patches, <i>Dissertation</i> , 2015, Universität Hamburg.
[21]	A. Fick, Ueber Diffusion, <i>Ann. Phys.</i> 170 (1855) 59 .
[22]	J. Crank, The Mathematics of Diffusion, 1975, Oxford University Press, New York, ISBN 0 19 853344 6.
[23]	W. R. Vieth, Diffusion In and Trough Polymers, 1979, Oxford University Press, New York, ISBN 3-446-15574-0.
[24]	S. Wittchen, H. Kahl, D. Waltschew, I. Shahzad, M. Beiner, V. Cepus, Diffusion Coefficients of Polyurethane Coatings by Swelling Experiments using Dielectric Spectroscopy, <i>J. Appl. Polym. Sci.</i> 137 (2020) 49174.
[25]	A. McIlhagger, D. Brown, B. Hill, The development of a dielectric system for the on-line cure monitoring of the resin transfer moulding process, <i>Compos. Part A Appl. Sci. Manuf.</i> 31 (2000) 1373–1381.
[26]	K. Zahouily, C. Decker. E. Kaisersberger, M. Gruener, Real-time UV cure monitoring, <i>Eur. Coating J.</i> 11 (2003) 245-249.
[27]	R. A. Pethrick, D. Hayward, Real time dielectric relaxation studies of dynamic polymeric systems, <i>Prog. Polym. Sci.</i> 27 (2002) 1983-2017.
[28]	M. G. Penon, S. J. Picken, M. Wübbenhorst, J. van Turnhout, Vapor Diffusion in Porous/Nonporous Polymer Coatings by Dielectric Sorption Analysis, <i>J. Appl. Polym. Sci.</i> 105 (2007) 1471-1479.
[29]	B. Gong, Y. Tu, Y. Zhou, R. Li, F. Zhang, Z. Xu, D. Liang, Moisture Absorption Characteristics of Silicone Rubber and Its Effect on Dielectric Properties, <i>Annual Report Conference on Electrical Insulation and Dielectric Phenomena</i> (2013) 430-433.
[30]	L. Ollivier-Lamarque, M. Lallart, N. Mary, T. Uchimoto, S. Livi, S. Marcelin, H. Miki, Dielectric Analysis of Water Uptake in Polymer Coating using Spatially Defined Fick's Law and Mixing Rule, <i>Prog. Org. Coat.</i> 148 (2020) 105846.
[31]	https://dupont.com , Liveo™ BIO-PSA 7-4201 silicone adhesives, last accessed 27 th November 2023.
[32]	https://dupont.com , Liveo™ BIO-PSA 7-4301 silicone adhesives, last accessed 27 th November 2023.
[33]	https://dupont.com , Liveo™ BIO-PSA 7-4501 silicone adhesives, last accessed 27 th November 2023.

[34]	https://dupont.com , Liveo™ BIO-PSA 7-4601 silicone adhesives, last accessed 27 th November 2023.
[35]	https://www.3m.com , 3M™ Scotchpak™ Polyester Backing Film Laminate, 9732, last accessed 20 th November 2023.
[36]	M. Meurer, R. Kádár, E. Ramakers-van Dorp, B. Möglinger, B. Hausnerová, Nonlinear oscillatory shear tests of pressure-sensitive adhesives (PSAs) designed for transdermal therapeutic systems (TTS). <i>Rheol. Acta</i> , 60 (2021) 553–570.
[37]	M. Meurer, L. Retterath, E. Ramakers-van Dorp, B. Möglinger, B. Hausnerová, Effects of resin content on water diffusion in two chemically different silicone based pressure sensitive adhesives (PSA) using dielectric analysis (DEA). Submitted to <i>APL Bioeng</i> , December 2023.
[38]	M. Meurer, T. Prescher, E. Ramakers-van Dorp, B. Möglinger, B. Hausnerová, RheoTack—An approach to investigate retraction rate dependent detaching behavior of pressure sensitive adhesives. <i>J. Rheol.</i> 66 (2022) 505-514.
[39]	M. Meurer, G. Kamsu, C. Dresbach, E. Ramakers-van Dorp, B. Möglinger, B. Hausnerová, Rate dependent tack behavior of silicone-based pressure sensitive adhesives for transdermal therapeutic systems. Submitted to <i>J. Ind. Eng. Chem.</i> November 2023
[40]	A.M. Wessendorf, D.J. Newman, Dynamic understanding of human skin movement and strain-field analysis. <i>IEEE Trans. Bio-Med. Eng.</i> 59 (2012) 3432–3438.
[41]	R. Maiti, L.C. Gerhardt, Z.S. Lee, R.A. Byers, D. Woods, J.A. Sanz-Herrera, S.E. Franklin, R. Lewis, S.J. Matcher, M.J. Carré, In vivo measurement of skin surface strain and sub-surface layer deformation induced by natural tissue stretching. <i>J. Mech. Behav. Biomed.</i> 62 (2016) 556–569.
[42]	W. Ge, A. Sfara, B. Hians, Skin deformation during shoulder movements and upper extremity activities. <i>Clin. Biomech.</i> 47 (2017)1–6.
[43]	H.G. Sim, K.H. Ahn, S.J. Lee, Large amplitude oscillatory shear behavior of complex fluids investigated by a network model: a guideline for classification. <i>J. Non-Newton. Fluid.</i> 112 (2003) 237–250.
[44]	F.J. Stadler, D. Auhl, H. Münstedt, Influence of the molecular structure of polyolefins on the damping function in shear. <i>Macromolecules.</i> 41 (2008) 3720–3726.
[45]	E.P. Chang, Viscoelastic properties of pressure-sensitive adhesives. <i>J. Adhesion.</i> 60 (1997) 233–248.
[46]	C.A. Dahlquist, Pressure sensitive adhesives. In: Patrick RL (ed) <i>Treatise on adhesion and adhesive</i> , vol 2, 1969, Marcel Dekker, New York, pp 219–260
[47]	M.A. Cziep, M. Abbasi, M. Heck, L. Arens, M. Wilhelm, Effect of molecular weight, polydispersity, and monomer of linear homopolymer melts on the intrinsic mechanical nonlinearity $3Q_0(\omega)$ in MAOS. <i>Macromolecules</i> 49 (2016) 3566–3579.
[48]	A. Fick, Ueber Diffusion, <i>Ann. Phys.</i> 170 (1855) 59 .
[49]	L. Du, M. Namvari, F. Stadler, Large amplitude oscillatory shear behavior of graphene derivative/poly-dimethylsiloxane nanocomposites. <i>Rheol. Acta</i> 57 (2018) 429–443.

[50]	M. Kamkar, E. Aliabadian, A.S. Zeraati, U. Sundaraj, Application of nonlinear rheology to assess the effect of secondary nanofiller on network structure of hybrid polymer nanocomposites. <i>Phys. Fluids</i> 30 (2018) 023102.
[51]	M. Kamkar, Large amplitude oscillatory shear flow: microstructural assessment of polymer nanocomposites, hydrogels, and interfaces. Dissertation, 2020, University of Calgary.
[52]	K. Gaska, R. Kádár, Evidence of percolated network at the linear - nonlinear transition in oscillatory shear. <i>AIP Conf. Proc.</i> 2107 (2019) 050003.
[53]	T.B. Goudoulas, N. Germann, Concentration effect on the nonlinear measures of dense polyethylene oxide solutions under large amplitude oscillatory shear. <i>J. Rheol.</i> 62 (2018) 1299–1317.
[54]	E. Aliabadian, S. Sadeghi, M. Kamkar, Z. Chen, U. Sundararaj, Rheology of fumed silica nanoparticles/partially hydrolyzed polyacrylamide aqueous solutions under small and large amplitude oscillatory shear deformations. <i>J. Rheol.</i> 62 (2018)1197–1216.
[55]	S. Khandavalli, J.P. Rothstein, Large amplitude oscillatory shear of three different shear-thickening particle dispersions. <i>Rheol. Acta</i> 54 (2015) 601–618.
[56]	Z. Wang, D.Z. Jia, H.M. Fang, C.Z. Guan, Absorption and Permeation of Water and Aqueous Solutions of High-temperature Vulcanized Silicone Rubber. <i>IEEE T. Dielect. El. In.</i> 22 (2015) 6.
[57]	K. Asaoka, S. Hirano, Diffusion coefficient of water through dental composite resin. <i>Biomaterials.</i> 24 (2003) 975-979.
[58]	K. Zahouily, C. Decker, E. Kaisersberger, M. Gruener, Real-time UV cure monitoring. <i>Eur Coating J</i> ,11 (2003) 245-9.
[59]	G.T. Fieldson, T.A. Barbari, The use of FTi.r.-a.t.r.spectroscopy to characterize penetrant diffusion in polymers. <i>Polymer.</i> 34 (1993) 1146-1153.
[60]	H. Lee, The Handbook of Dielectric Analysis and Cure Monitoring. Vol 156, 2017, Lambert Technol LLC, Boston, MA.
[61]	B. V. Zeghbroek, Principles of Semiconductor Devices. Prentice Hall, New Jersey, 2002.
[62]	A. K. Doolittle, Studies in Newtonian Flow II. The Dependence of the Viscosity of Liquids on Free-Space. <i>J. Appl. Phys.</i> 22 (1951) 1471-1475.
[63]	F.J. Millero, G.K. Ward, K.F. Lepple, E.V. Hoff, Isothermal compressibility of aqueous sodium chloride, magnesium chloride, sodium sulfate, and magnesium sulfate solutions from 0 to 45.deg. at 1 atm. <i>J. Phys. Chem.</i> 78 (1974) 1636-1643.
[64]	Y. Marcus, Electrostriction, Ion Solvation, and Solvent Release on Ion Pairing. <i>J. Phys. Chem. B.</i> 109 (2005) 18541-18549.
[65]	J.C. Hindman, Nuclear Magnetic Resonance Effects in Aqueous Solutions of 1–1 Electrolytes. <i>J. Chem. Phys.</i> 36 (1962) 1000-1016.
[66]	R. W. Impey, P.A. Madden, I.R. McDonald, Hydration and Mobility of Ions in Solution. <i>J. Phys. Chem.-US.</i> 87 (1983) 25.
[67]	R. Heyrovská, Ionic Concentrations and Hydration Numbers of “Supporting Electrolytes”, <i>Electroanal.</i> 18 (2006) 351-361.

[68]	Z. Wang, Z.D. Jia, M.H. Fang, Z.C. Guan, Absorption and Permeation of Water and Aqueous Solutions of High-temperature Vulcanized Silicone Rubber. <i>IEEE T Dielect. El. In.</i> 22 (2015) 6.
[69]	J. Zhang, J. Cui, F. Wang, J. Xiang, Z. Cao, Q. Wang, Diffusion in Aqueous Solutions with Multivalent Cations and Especially in Cationic First Hydration Shell. <i>J. Phys. Chem. B.</i> , 126 (2022) 3585-3592.
[70]	A. Chiche, P. Pareige, C. Creton, Role of surface roughness in controlling the adhesion of a soft adhesive on a hard surface. <i>C. R. Acad- Sci. Paris.</i> 1 (2000) 1197-1204.
[71]	C. Creton, M. Cicotti, Fracture and adhesion of soft materials. <i>Rep. Prog. Phys.</i> 79 (2016) 046601.
[72]	K. Takahashi, O. Ryuto, K. Inaba, K. Kishimoto, Scaling effect on the detachment of pressure-sensitive adhesives through fibrillation characterized by a probe-tack test. <i>Soft Matter.</i> 16 (2020) 6493-6500.
[73]	M.A. Droesbeke, A. Simula, J.M. Asua, F.E. Du Prez, Biosourced terpenoids for the development of sustainable acrylic pressure-sensitive adhesives via emulsion polymerization. <i>Green Chem.</i> 22 (2020) 4561.
[74]	K. Takahashi, M. Shimizu, K. Inaba, K. Kishimoto, Y. Inao, T. Sugizaki, Tack performance of pressure-sensitive adhesive tapes under tensile loading. <i>Int. J. Adhes. Adhes.</i> 45 (2013) 90-97.

LIST OF FIGURES

Fig. 1	Design of transdermal therapeutic systems (TTS) – a) drug-in-adhesive matrix type and b) drug reservoir type [2].
Fig. 2	Chemical structures of the non-amine compatible (NAC) and amine-compatible (AC) PSA and the steps of their synthesis (according to [9]).
Fig. 3	Scheme of TTS manufacturing with a coating head, drying zone and laminating zone (according to [10]).
Fig. 4	Scheme of the oscillatory shear measurement a) sample is loaded in an oscillatory manner between two plates, b) sinusoidal excitation (γ), response signal (τ) and phase angle(δ).
Fig. 5	G' and G'' being independent from strain amplitude γ_0 in the LVE or SAOS region and dependent from the strain amplitude γ_0 in the middle and large amplitude oscillatory shear region (MAOS, LAOS).
Fig. 6	Normalized elastic a) and viscous b) Lissajous-Bowditch diagrams for linear viscoelastic behavior (light grey) and nonlinear behavior (green) with determination of zero-strain modulus G'_M , maximum strain modulus G'_L , zero-rate dynamic viscosity η'_M , and maximum-rate dynamic viscosity η'_L .
Fig. 7	Effect of temperature on the ion viscosity during desorption [24].
Fig. 8	Strain amplitude dependent storage G' and loss moduli G'' of AC- and NAC-PSAs for $\omega = 1$ rad/s; symbols = measured data; lines = Carreau-Yasuda-like fits [36].

Fig. 9	Representation according to Chang and Dahlquist of SAOS data from AC- and NAC-PSAs [36].
Fig. 10	Strain amplitude dependent nonlinear parameter $I_{3/1}$ (γ_0) for AC- and NAC-PSAs [36].
Fig. 11	Strain amplitude and frequency dependent strain stiffening ratios S for AC- and NAC-PSAs [36].
Fig. 12	Strain amplitude and frequency dependent shear thickening ratios T for AC- and NAC-PSAs [36].
Fig. 13	Cross sectional sketch of the experimental setup with a temperature controlled metal block, sealing, the dielectric analysis mini IDEX-sensor, the fringe field of the DEA sensor, the PSA-film and the applied diffusant on the PSA-film a), stacked PSA-films are positioned on the mini-IDEX sensor, enclosed by the sealant b), water-temperature controlled aluminum-block with PTFE-covering plate, added onto the mini-IDEX sensor setup [37].
Fig. 14	Time dependent η^{ion} -time curve from the DEA to monitor the process of diffusing water into a silicone PSA, with characteristic evaluated points [37].
Fig. 15	Ion viscosity (η^{ion}) as a function of time (t) for various film thickness of AC and b) NAC PSA-films (resin content of $v_F = 51.6$ %) [37].
Fig. 16	Influence of the resin content and the PSA-film thickness of AC a) and NAC PSA-films b) [37].
Fig. 17	Influence of the diffusant and the PSA-film thickness of AC a) and NAC PSA-films b) [37].
Fig. 18	Resin content dependent results from probe tack a) and peel adhesion strength testing for AC- and NAC-TTS.
Fig. 19	Sketch of the <i>RheoTack</i> approach with the upper plate as the probe rod, the temperature module plate (TMP) for patch fixation as the lower plate, and the implemented optical observation unit for synchronized video monitoring from the bottom (90 °, camera 1), lateral (0°, camera 2), and top (45°, camera 3) to the rheometer [38].
Fig. 20	Evaluation of F - h curve with deformation phases and characteristic <i>RheoTack</i> quantities: S , $F_{\text{start fib}}$, $h_{\text{start fib}}$, $E_{\text{start fib}}$, F_{max} , h_{max} , E_{adh} and corresponding structures at $F_{\text{start fib}}$, and F_{max} (NAC-TTS) [38].
Fig. 21	Mean force F - h curves from <i>RheoTack</i> testing at retraction speeds of 0.01, 0.1 and 1 mm/s obtained for five different TTS samples (NAC-TTS 49.1 %) [38].
Fig. 22	F - h curves of AC- and NAC-TTS with $v_F = 54.2$ %, 51.6 % and 49.1 %, tested with retraction speed of $v_{\text{retract}} = 0.1$ mm/s with P8 [39].
Fig. 23	Starting situation of the rods P8, P5 and R5 with the corresponding displacement and inclination angles at the end of the dwell time for NAC-TTS, $v_F = 49.1$ % [39]
Fig. 24	Normalized F - h -curves (to P5) of P8, P5 and R5 for AC- (top) and NAC-TTS (bottom) with $v_F = 49.1$ % [39].
Fig. 25	State of bonding for P8 a), P5 b), and R5 c) at h_{max} (NAC-TTS, $v_F = 49.1$ % and $v_{\text{retract}} = 0.01$ mm/s) with stretching patterns of the backing layer between the TMP and rods, the resulting angles of the TTS between TMP and rods: α for P8, β for P5

	and γ for R5, and the TTS's retraction at the TMPs bottom from initial edge of TTS R_{TTS_0} to the resulting edge of TTS R_{TTS} [39].
Fig. 26	Deformation structures as the stretching patterns of the TTS and cavity sizes observed with camera 1 under the probe rod in 90° , a) $v_{retract} = 0.01$ mm/s, b) $v_{retract} = 0.1$ mm/s, c) $v_{retract} = 1$ mm/s [38].
Fig. 27	Flow chart of the contribution to science and practice employed in the PhD. thesis [10].

LIST OF TABLES

Table 1	Pros and cons of PSAs that are used for TTS [6-8].
Table 2	Composition of PSA samples used. [31-34]
Table 3	Measured properties, determined quantities, tested samples and instruments.
Table 4	Resin content dependent thickness averages of parameter A , parameter B and diffusion coefficients D of AC- and NAC-PSAs [37].
Table 5	Retraction speed dependent compression times [39].
Table 6	Rod geometries used with their dimensions and surface roughness's (grid distance = 5 mm) [39].

ABBREVIATIONS

AC	Amine compatible
API	Active pharmaceutical ingredients
CTE	Coefficient of thermal expansion
DEA	Dielectric analysis
EMA	European Medicines Agency
EVA	Ethylene vinyl acetate
FDA	Food and Drug Administration
ICH	International Council on Harmonisation of Technical Requirements for Registration of Pharmaceuticals for Human Use
IDEX	Interdigitated electrode
LAOS	Large amplitude oscillatory shear
LVE	Linear viscoelastic region
TTS	Transdermal therapeutic systems
MAOS	Middle amplitude oscillatory shear
NAC	Non-amine compatible
PDMS	Polydimethylsiloxane
PET	Polyethylene terephthalate
PSA	Pressure sensitive adhesive
PU	Polyurethane
PTFE	Polytetrafluoroethylene
SAOS	Short amplitude oscillatory shear
TMP	Temperature module plate

Symbols

A	Contribution of the final ion concentration to the ion viscosity
A_{contact}	Contact area
A_{P5}	Contact area of P5
A_{P8}	Contact area of P8
A_{R5}	Contact area of R5

A_0	Pre-exponential factor
B	Doolittle constant
B'	Fractional free volume
c_{ion}^0	Initial ion concentration
c_{∞}^{PSA}	Final water concentration in the PSA
C_1	Transition factor from linear to nonlinear viscoelastic region
C_2	Range of the transition factor
C_3	Strain amplitude dependency of G' and G'' within the nonlinear range
d_{max}	$3d_{\text{penetration}}$ = the sensitivity range of the mini IDEX sensor
d_{PSA}	Thickness of the PSA-layer
D	Diffusion coefficient
D_{con}	Contact diameter
D_{sphere}	Diameter of the sphere
D_{TMP}	TMP diameter
E_{adh}	Adhesion energy
$E_{\text{start fib}}$	Activation energy of cavity and/or fibril formation
E''	Loss modulus
f	Frequency
$F(h)$	Force
F_{max}	Maximum force
$F_{\text{start fib}}$	Initiation force of cavity and/or fibril formation
G^*	Complex shear modulus
G'	Storage modulus
G'_0	Initial storage moduli
$G'_M(\gamma)$	Zero-strain modulus
$G'_L(\gamma)$	Maximum-strain modulus
G''	Loss modulus
h	Retraction displacement

h_{\max}	Retraction displacement at F_{\max}
$h_{\text{start fib}}$	Retraction displacement at $F_{\text{start fib}}$
I_1	1 st harmonic from Fourier analysis
I_3	3 rd harmonic from Fourier analysis
I_5	5 th harmonic from Fourier analysis
$I_{3/1}$	Ratio of 3 rd and 1 st harmonic from Fourier analysis
k_2	Constant
K_2	Constant
M_{∞}	Relative mass at saturation
m_{∞}	Saturation level of water uptake
P5	Rod with $\varnothing = 5$ mm
P8	Rod with $\varnothing = 8$ mm
R _{TTS}	Resulting TTS edge
R _{TTS,0}	Initial edge of TTS
R5	Rounded shaped rod with $\varnothing = 5$ mm and $D_{\text{sphere}} = 5$ mm
$S(\gamma_0)$	Strain stiffening ratio
S	Stiffness
$\tan(\delta)$	Loss factor
T_g	Glass transition temperature
$T(\gamma_0)$	Shear thickening ratio

Greek symbols

$\alpha_{L,G}$	Coefficient of thermal expansion in the glassy state, before T_g
$\alpha_{L,L}$	Coefficient of thermal expansion in the liquid state, after T_g
$\gamma_0(\omega)$	Deformation amplitude

γ_{0C}	Limit of LVE
$\dot{\gamma}(t)$	Time dependent shear rate
$\dot{\gamma}_0$	Shear rate amplitude
δ	Phase angle
ε''	Dielectric loss
ε_0	Dielectric constant
$\eta^{\text{ion}}(f, t)$	Ion viscosity dependent on frequency or time
η_0^{ion}	Constant initial ion viscosity
$\eta_{\infty}^{\text{ion}}$	Final ion viscosity
$\eta_{\tau 25\%}^{\text{ion}}$	Ion viscosity, 25 % below η_0^{ion}
$\eta_{\tau 63\%}^{\text{ion}}$	Ion viscosity, 63 % below η_0^{ion}
$\eta'_M(\dot{\gamma})$	Zero-rate dynamic viscosity
$\eta'_L(\dot{\gamma})$	Maximum-rate dynamic viscosity
ν_F	Resin content
ν_{retract}	Retraction speed
ν_{free}	Relative free volume
ρ_{solv}	Density of the solvent
σ	Ion conductivity
$\tau(\dot{\gamma})$	Shear stress
τ_{diff}	Diffusion time constant
$\tau_{25\%}$	Time at $\eta_{\tau 25\%}^{\text{ion}}$
$\tau_{63\%}$	Time at $\eta_{\tau 63\%}^{\text{ion}}$
ω	Angular frequency

PUBLICATIONS, POSTERS AND PRESENTATIONS

Publications in a context of this doctoral work:

- Michael Meurer, Roland Kádár, Esther Ramakers-van Dorp, Bernhard Möglinger, Berenika Hausnerová, **Nonlinear oscillatory shear tests of pressure-sensitive adhesives (PSAs) designed for transdermal therapeutic systems (TTS)**. *Rheol. Acta* 2021, 60, 553–570.
- Michael Meurer, Tim Prescher, Esther Ramakers-van Dorp, Bernhard Möglinger, Berenika Hausnerová, **RheoTack—An approach to investigate retraction rate dependent detaching behavior of pressure sensitive adhesives**. *J. Rheol.* 2022, 66, 505-514.
- Michael Meurer, Gatien Kamsu, Christian Dresbach, Esther Ramakers-van Dorp, Bernhard Möglinger, Berenika Hausnerová, **Rate dependent tack behavior of silicone-based pressure sensitive adhesives for transdermal therapeutic systems**. Submitted to *J. ind. Eng. Chem.* November 2023.
- Michael Meurer, Lucca Retterath, Esther Ramakers-van Dorp, Bernhard Möglinger, Berenika Hausnerová, **Effects of resin content on water diffusion in two chemically different silicone based pressure sensitive adhesives (PSA) using dielectric analysis (DEA)**. Submitted to *APL Biong.* December 2023.

Conference Publications:

- **Improved Tack-Measurements of Transdermal Therapeutic System**, *Annual European Rheology Conference*, Portoroz, Slovenia, April 2019, poster presentation.
- **Nonlinear oscillatory shear tests of Pressure Sensitive Adhesives designed for Transdermal Therapeutic Systems**, *Nordic Rheology Conference*, Gothenburg, Sweden 2019, oral presentation.
- **Large Amplitude Oscillatory Shear Tests of Pressure Sensitive Adhesives Designed for Transdermal Therapeutic Systems**, *International Congress on Rheology*, online (Rio de Janeiro, Brazil), 2020, oral presentation.
- **RheoTack - a new comprehensive tack test method for adhesive tapes**, *Times of Polymer and Composites*, Ischia, Italy 2021, oral presentation.
- **RheoTack - rate dependent tack behavior of pressure sensitive adhesives – effect of composition and probe geometry**, *20th ICEM International Conference on Experimental Mechanics*, Porto, Portugal 2022, oral presentation.

CURRICULUM VITAE

Date and place of birth June 9th, 1987 in Andernach, Germany
Permanent address University of Applied Sciences Bonn-Rhein-Sieg
Von-Liebig-Str. 20
D-53359 Rheinbach, Germany
Tel: (+49) 2241 865 755
E-mail: Michael.Meurer@h-brs.de

Education

since 10/2017 **Ph.D. studies at Tomas Bata University in Zlín,**
Faculty of Technology, Department of Production
Engineering

09/2011 – 10/2013 **M.Sc. Applied Polymer Sciences, FH-Aachen-**
University of Applied Sciences,
Department of Chemistry and Biotechnology

09/2008 – 05/2011 **B.Sc. Chemistry with material sciences at**
University of Applied Sciences Bonn-Rhein-Sieg,
Department of Natural Sciences

Work experience

Since 08/2016 **Scientific assistant at University of Applied**
Sciences Bonn-Rhein-Sieg, Rheinbach,
Faculty of Applied Sciences

Since 09/2017 **Management board within the TREE-institute,**
University of Applied Sciences Bonn-Rhein-Sieg,
Rheinbach and St. Augustin

01/2014-08/2016 **Product development engineer, AKRO-**
PLASTIC GmbH, Niederzissen, Germany

Michael Meurer, Ph.D.

**Testing of Pressure Sensitive Adhesives
for Transdermal Therapeutic Systems**

**Testování adheziv v transdermálních terapeutických
materiálech**

Doctoral Thesis Summary

Published by: Tomas Bata University in Zlín,
nám. T. G. Masaryka 5555, 760 01 Zlín.

Edition: published electronically

Typesetting by: Michael Meurer, Ph.D.

This publication has not undergone any proofreading or editorial review.

Publication year: 2024

First Edition

ISBN 978-80-7678-230-3

